12-2021

Synthesis of Phosphatidylethanolamine Lipids for Model Studies of the Cell Membrane

John Hayford G. Teye-Kau
East Tennessee State University

Synthesis of Phosphatidylethanolamine Lipids for Model Studies of the Cell Membrane

---

A thesis

presented to

the faculty of the Department of Chemistry

East Tennessee State University

In partial fulfillment

of the requirements for the degree

Master of Science in Chemistry

---

by

John Hayford Gbebi Teye-Kau

December 2021

Dr. Robert F. Standaert, Ph.D., Chair

Dr. Abbas G. Shilabin, Ph. D.

Dr. Gregory W. Bishop, Ph. D.

Keywords: cell membrane, fatty acids, phospholipids, phosphatidylglycerol (PG), phosphatidylethanolamine (PE), phosphatidylcholine (PC)

ABSTRACT

Synthesis of Phosphatidylethanolamine Lipids for Model Studies of the Cell Membrane

by

John Hayford Gbebi Teye-Kau

Concerns about global warming have resulted in a surge of research into alternatives to fossil fuels. In recent years, biofuels have gained traction due to their low environmental impact. Biofuel production most commonly employs microorganisms to convert biomass to fuel for industrial and transportation applications. Compounds made in biofuel production, however, are toxic to cell membranes and disrupt their integrity, harming the microorganisms and limiting biofuel yield. A key to overcoming this challenge is understanding how fuels interact with microorganisms' cell membranes, which perform a host of functions, including transport, cell recognition, transduction, and movement. Phospholipids are the cell membrane's building blocks and provide the critical matrix to support these vital functions. This research sought to make in-vitro membrane phospholipid models of the bacterium *Bacillus subtilis* (a biofuel producer candidate), subject them to fuel stress and employ fluorescence techniques to understand how fuels affect membrane integrity.

DEDICATION

This work is dedicated to my parents, family, and loved ones who have been part of my success story.

ACKNOWLEDGMENTS

I would like to express my heartfelt gratitude to Dr. Robert F. Standaert, my research advisor, for the opportunity to be a part of his research group, the mentorship, guidance, and patience throughout this journey.

I would like to thank Dr. Abbas Shilabin and Dr. Gregory Bishop for accepting to be a part of my Advisory Committee. I am grateful for their help with my thesis.

I would like to say thank you to Dr. Reza Mohseni as well, for his help with instrumentation and analysis for my work.

I am grateful to Ms. Maria Kalis for her help in administrative and organizational aspects throughout my graduate schoolwork.

I appreciate the support of Apostle Dr. Arnold Nyarambi and his wife Pastor Dumisa Nyarambi for their support and prayers for me throughout my stay and study in ETSU.

I would also like to thank Haley Bell, and my research colleagues for their help and support during the entire project.

Special gratitude to East Tennessee State University for funding support for this research.

TABLE OF CONTENTS

LIST OF FIGURES

LIST OF ABBREVIATIONS

CL	Cardiolipin
DCC	*N*,*N'*-Dicyclohexylcarbodiimide
DCM	Dichloromethane
DI	Deionized
DIPEA	*N*,*N*-Diisopropylethylamine
DMAP	*N*,*N*-Dimethyl aminopyridine
DMF	4-Dimethyl formamide
DPH	1,6-Diphenyl-1,3,5-hexatriene
DPPC	Distearoyl phosphatidylcholine
DSC	Differential scanning calorimetry
DTCC	Dilithium tetrachlorocuprate
ESR	Electron spin resonance
FA	Fatty acid
FAME	Fatty acid methyl ester
FRET	Förster or fluorescence resonance energy transfer
GC	Gas chromatography
GC–MS	Gas chromatography–mass spectrometry
GP	Generalized polarization
MCPBA	*meta*-Chloroperbenzoic acid
NMR	Nuclear magnetic resonance
PA	Phosphatidic acid
PC	Phosphatidylcholine
PE	Phosphatidylethanolamine
PG	Phosphatidylglycerol
POPE	1-Palmitoyl-2-oleoyl phosphatidylethanolamine
POPG	1-Palmitoyl-2-oleoyl phosphatidylglycerol
SDP	Scattering density profile

sn	Stereospecific numbering
SOPG	1-Stearoyl-2-oleoyl phosphatidylglycerol
THF	Tetrahydrofuran
TFA	Trifluoroacetic acid
TLC	Thin layer chromatography
t_R	Retention time
UV	Ultraviolet

CHAPTER 1. INTRODUCTION

The Cell Membrane

The cell is the most basic unit of life. Cells consist of complex biochemical systems that need to be protected and separated from their outside environment. A cell always has a plasma (cell) membrane, and certain types of bacteria (Gram-negative) have a second, outer membrane, or an additional partition that functions as a boundary between the cell and its environment. Higher organisms (eukaryotes) have multiple membrane-bound organelles inside their cells. The cell membrane is composed of a thin and flexible hydrophobic film[1] embedded with thousands of carbohydrates, proteins, and lipids. The membrane has an amphipathic phospholipid (glycerophospholipid) bilayer which forms in an aqueous environment and is very important in the general structure. The phospholipids are the most abundant components found in the bilayer,[2] and they form a physical barrier that concentrates and localizes materials and molecules in the cytoplasm from the cell's external environment.[3] These lipids have unique properties and can perform individual functions. The unique composition of the cell membrane plays a major role in determining its functionality. One major function of the cell membrane is to selectively permit certain substances (most importantly, nutrients) into the cell, and to export toxic waste out of the cell.[1] The admission or rejection of a substance from a cell depends on the composition and thickness of the membrane, with the membrane itself serving as a barrier to polar molecules but having embedded protein transporters for a wide range of substances. Another function of the cell membrane is to identify foreign bodies and to recognize self-cells.[4] The cell membrane can also function in multiple pathways of signal transduction (cellular communication).[5–7] A lot of research has been done on the cell membrane and many models have been proposed to describe the cell membrane.

Early Models of the Cell Membrane

Studies of the cell membrane, or plasma membrane (plasmalemma) saw little light before the pauci molecular model was proposed by Hugh Davson and James Danielli in 1935. This model describes the membrane as a bilayer of phospholipids sandwiched between layers of peripheral or functional globular proteins.[8]

In 1972, the fluid mosaic model was proposed by G. Nicolson and S. J. Singer (also known as the Singer–Nicolson or S–N model). This new model postulated a fluid-phase phospholipid bilayer embedded with proteins that provided various functions to the membrane. The mosaic-like domain structure of the cell membrane can explain how the diffusion rate of different molecules depends on the structure (length, unsaturation and branching) of the fatty acid chains of the lipid bilayer.[9]

Figure 1 shows a cross-section of a membrane as described by the S–N model. The dark circles on the top and bottom of the figure represent polar head groups of phospholipids. The wavy lines, or "tails" of the phospholipids, represent the long-chain fatty acids (FAs) of the phospholipids in the bilayer.[8] The S–N model explains the hydrophobic and hydrophilic interactions of the bilayer.[10–12] The polar head groups maintain contact with water (the aqueous medium of the cytoplasm or outside environment of the cell), while the nonpolar long-chain fatty acids cluster away from aqueous contact. The globular proteins (with hydrophobic surfaces exposed to the tails and polar, charged surfaces exposed to heads and water) in this model are embedded within the lipid bilayer, which serves as a matrix or solvent for them and allows them to diffuse freely in the plane of the membrane.[9,13]

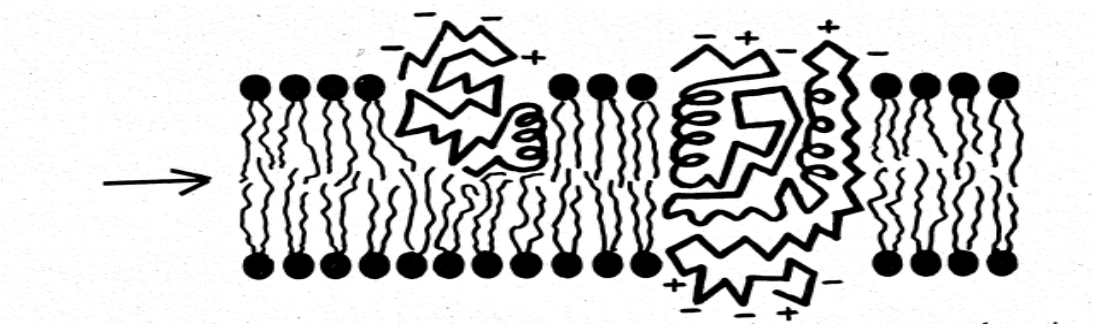

Figure 1. A cross-section of the fluid mosaic model of membrane structure. Copyright American Association for the Advancement of Science, used with permission

Updated Cell Membrane Model

Contemporary models of the cell membrane propose the existence of specialized membrane domains (sometimes termed lipid rafts) and protein complexes. While the existence of non-homogeneity in the fluid mosaic had long been postulated, the lipid raft hypothesis was formalized by Kai Simons, Elina Ikonen, and Thomas Harder in 1997.[7,14,15] Lipid rafts are composed of cholesterol and specialized types of phospholipids in a distinct liquid-ordered phase, dispersed in a liquid-disordered matrix made of unsaturated glycerol phospholipids. The concept of lipid rafts provides a framework to explain how membranes carry out many vital biological functions. Lipid rafts can include or exclude different transmembrane proteins. Some may reside in the raft only for a limited period of time in the execution of a particular function.[14] Rafts thus serve to organize multiprotein complexes in signal transduction.

Some of the significant conclusions that have been drawn from studying membranes over the last 50 years are as follows:[15–17]

1. The physical properties and functions of membranes are dependent on the lipids, their associated proteins, and the integrity of their assembly.[17]

2. The hydrophobicity of the fatty acid tails provides an excellent, selectively permeable barrier that is totally impermeable to charged and polar molecules but allows passage of water and small, hydrophobic or weakly polar molecules.

3. The ability of the membrane to adapt to various environments is largely a result of hydrocarbon tail structure variations.[2]

4. Lipid rafts are believed to facilitate signal transduction and membrane trafficking.[14]

5. Proteins can be excluded or included to flexible extents within lipid rafts.[14]

6. The function of some transmembrane proteins in lipids rafts is not well known, but the mutational investigations found that amino acids near the exoplasmic regions are critical.[14,18]

Membrane Phospholipids

The dominant constituents of the cell membrane are phospholipids and proteins, with the lipids forming the fundamental barrier itself and providing a matrix for the proteins.[9,13] Phospholipids are made of a glycerol "backbone" molecule with esterified fatty acids at positions *sn*-1 and *sn*-2 (stereospecific numbering 1 and 2), and a phosphate moiety at position *sn*-3 (stereospecific numbering 3), where the phosphate group may be free (forming a phosphatidic acid, IUPAC name 1,2-diacyl-*sn*-glycero-3-phosphate)[19] or esterified to one of several alcohols. Figure 2 shows a representative phosphatidylcholine (PC) lipid, where the phosphate is esterified with choline. PC lipids are common in plants and animals.

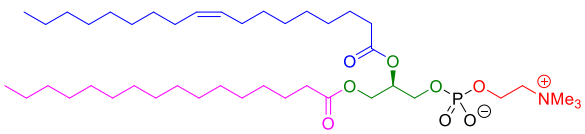

Figure 2. A phosphatidylcholine lipid. Color codes: magenta and blue, fatty acyl chains at positions *sn*-1 and *sn*-2, respectively; green, glycerol backbone; black, phosphate group at *sn*-3; and red, choline moiety

Phospholipids may form micelles or vesicles (spherical bilayers, Figure 3) depending on their structure. A micelle is a lipid molecule that has aggregated with the head groups in contact with an aqueous medium and the tails clustering together away from the aqueous medium. This arrangement is common to fatty acid salts (soaps) and phospholipids with a single fatty-acid tail (lyso lipids). Most phospholipids with two fatty-acid tails form bilayers rather than micelles. A lipid vesicle is made up of one (unilamellar) or more (multilamellar, like an onion) lipid bilayers in the form of a closed sphere. Vesicles are stable in an aqueous environment and can exist for a long period.[20] Micelles and especially vesicles have been used extensively as models in the study of the cell membrane. The self-assembly of a lipid bilayer is shown schematically in Figure 4.

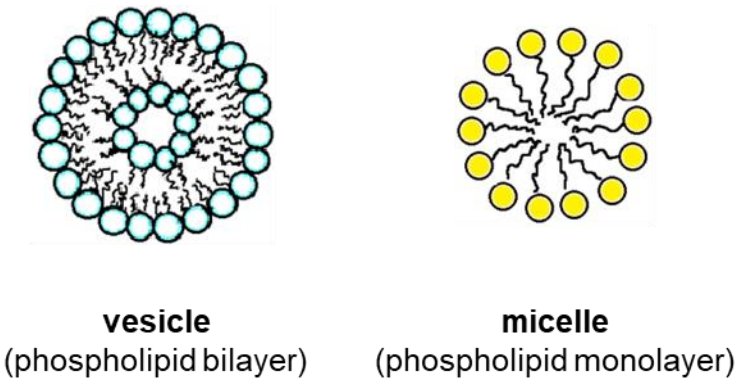

Figure 3. Supramolecular arrangements of phospholipid molecules in bilayers and micelles

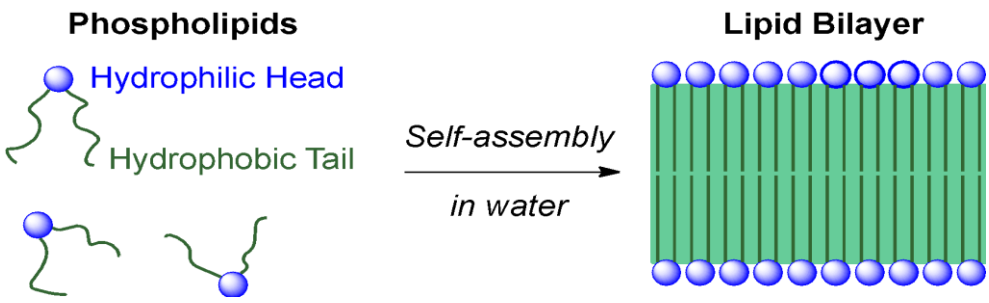

Figure 4. Phospholipid bilayer self-assembly in an aqueous environment. The hydrophobic tails align facing each other away from water, and the hydrophilic head groups face the aqueous environment. Image copyright Robert F. Standaert, used with permission

Bacterial Membrane Phospholipids

Bacteria are classified into two groups, Gram-positive and Gram-negative, based on their cellular anatomy.[3] Gram-positive bacteria have a single bilayer membrane surrounding the cytoplasm. Gram-negative bacteria have two distinct bilayer membranes, an inner plasma membrane and an outer membrane. Both Gram-positive and Gram-negative bacteria have a cell wall.[7] Phospholipids present in the bacterial membrane include phosphatidic acid (PA), phosphatidylglycerol (PG), phosphatidylethanolamine (PE), and cardiolipin (CL),[21] with Gram-positive organisms using mostly branched fatty acyl chains[27] instead of unsaturation to modulate fluidity (Figure 5).

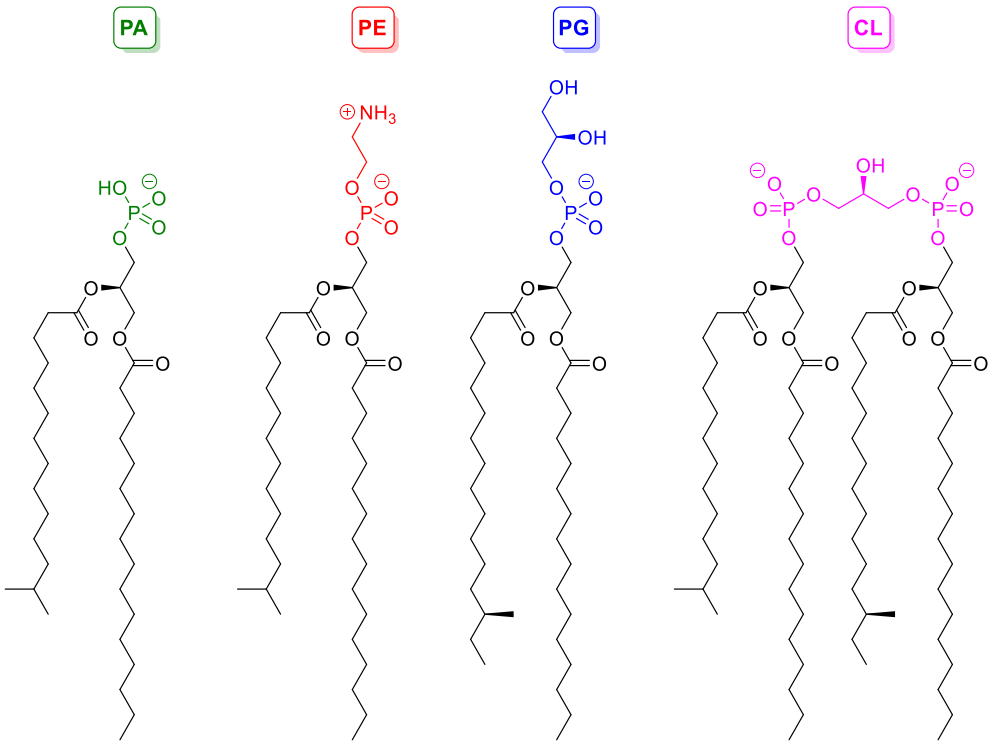

Figure 5. Representative Gram-negative bacterial membrane phospholipids. Phosphatidylethanolamine (PE) and phosphatidyglycerol (PG) lipids are most abundant. Cardiolipin (CL) is a dimer of PG. The fatty acyl chains vary in length, branching and location of the branch, if present

The nature of the acyl chain in the bacterial membrane lipid molecule determines to a large extent the biophysical properties of the lipid bilayer, in particular how thick and viscous it is. Viscosity must be maintained to control permeability to molecules, active solute transport, membrane protein function and other key properties.[12] The chain length mainly ranges between fourteen (14) and twenty (20) carbons. Bacteria adjust their fatty acid composition to maintain the membrane's biophysical properties and optimize growth at different temperatures and in response to stressors.[12]

Membrane Fluidity

Membrane fluidity refers to the viscosity of the lipid bilayer and the freedom of motion of the phospholipids in the membrane.[22–24] Phospholipid composition and packing affect membrane fluidity. The space occupied by the acyl chain and the phospholipid head group determine the freedom of motion each molecule is permitted.[23] The packing density of phospholipids in the membrane may be affected by proteins, pH,[22] carbohydrate content, certain cations (Ca^{2+}), or water.[23] Temperature may also affect membrane fluidity — increasing temperature increases fluidity, and decreasing temperature decreases fluidity.[24]

There are two main phases of the lipid bilayer: the gel phase (low fluidity) and the liquid crystalline phase (high fluidity), Figure 6. The liquid crystalline phase can be sub-divided into liquid disordered and liquid ordered, with the latter corresponding to membrane domains or lipid rafts. The liquid crystalline phase supports protein function and allows free diffusion within the bilayer.[24] In the gel phase, lipids pack together, forming an ordered, viscous state that impedes diffusion,[24] and the area per lipid decreases sharply, for example from ~65 $Å^2$ to 55 $Å^2$ with the model lipid distearoyl phosphatidylcholine (DPPC).[25] Diffusion coefficients in the gel phase are about 3 orders of magnitude lower than in the liquid disordered phase,[26] and cells require the fluidity of the liquid phase to function properly.

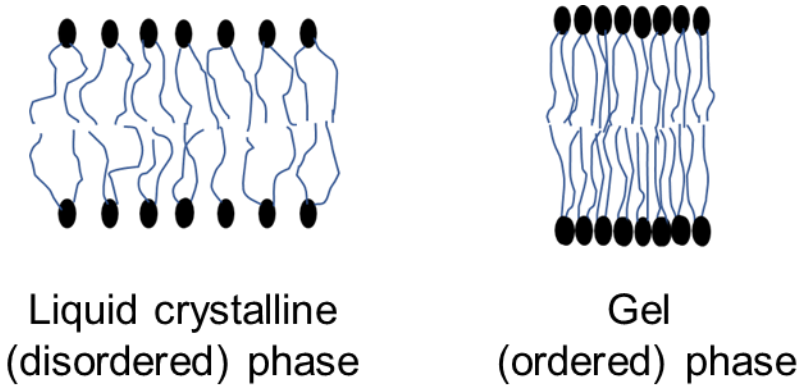

Figure 6. Membrane phases: liquid crystalline and gel phases. Adapted from Fonseca et al., 2019[24]

Bacteria restore balance in their membrane fluidity after environmental disturbances by altering fatty acyl chain structure. Rebalancing may be achieved by changing the types and ratios of branching and saturation in the acyl chain, or by varying the acyl chain length.[22,23] Saturation and lengthening of acyl chains increases the melting point of the membrane and decreases fluidity. *Cis* unsaturation introduces kinks that inhibit close packing and make the chains spread apart, increasing the area per lipid and increasing fluidity. Branching provides an alternative means of decreasing packing efficiency and increasing fluidity.[12,23,24] Gram-positive bacteria employ methyl branches at the penultimate or antepenultimate carbon of the fatty acyl chain (iso- and anteiso-fatty acids, respectively).

Cell Membrane Thickness

Modern technological advances have allowed researchers to study membrane composition, fluidity, bilayer thickness, and lipid area. Determining lipid structure, dynamics, and membrane thickness, however, has been a technical challenge.[6,27] Membrane thickness, in particular, is a measurement critical to better understanding specific membrane functions (e.g.,

transport of molecules in and out of the cell).[18] Recent work to determine the thickness of the acyl chains has been done using combined X-ray and neutron scattering data.[28]

In the research of Kučerka and co-workers, fully hydrated fluid-phase phospholipid bilayers of phosphatidylglycerol (PG)[29,30] and phosphatidylcholine (PC)[31,32] were studied. The scattering density profile (SDP) model was used to co-refine data from neutron scattering, X-ray scattering, and molecular dynamics simulations. The SDP model provides volume probabilities for each lipid component, leading to a natural definition of bilayer thickness in terms of the Gibbs dividing surface as the boundary of the central hydrocarbon region. The boundary is where the volume probability for the hydrocarbon part of the phospholipid crosses 0.5. Measured from the center of the bilayer, the thickness is denoted D_C, and the full hydrocarbon layer thickness as $2D_C$. For the model lipid 1-palmitoyl-2-oleoyl PG (POPG), $2D_C$ was found to be 27.7 Å at 30 °C. There is another Gibbs dividing surface at the water interface, where the volume probability for water crosses 0.5. This surface is used to define the overall membrane thickness D_B (also called the Luzzati thickness), and it was found to be 36.5 Å at 30 °C for POPC. There is only one *in-vivo* study, in which the hydrocarbon thickness of the *Bacillus subtilis* plasma membrane was determined to be 24.3 ± 0.9 Å.[18]

Determination of Membrane Fluidity

Evaluating membrane fluidity can help in understanding the impact of different stresses on the membrane. Membrane fluidity can be evaluated through a variety of techniques including differential scanning calorimetry (DSC), spectroscopic monitoring of fluorescent probes, electron spin resonance (ESR), nuclear magnetic resonance (NMR), and X-ray diffraction.[23,33] Fluorescence techniques in particular are useful to determine the average phase transition of the membrane.[22–24] Fluorescence polarization employs membrane-soluble probes as biological

markers[23] to monitor lipid structure and motion under stress conditions.[24] In a gel or crystalline environment, molecular motions are restricted, and fluorophores excited with polarized light emit substantially polarized light. In a fluid environment, rotation of the probe results in depolarization, i.e., emission of light in all directions.[22,23] These probes are dyes that may or may not partition themselves into the hydrocarbon layer, with accompanying changes in the fluorescence intensity.[33] Fluorescence anisotropy is independent of intensity, making it a useful property for fluidity analysis.[22]

In other cases, changes in emission wavelength can be used to understand the membrane environment. Laurdan (2-(dimethylamino)-6-lauroylnaphthalene)[34] is an environmentally sensitive probe[35] that can be excited in the ultraviolet (UV) region.[35,36] Laurdan (Figure 7) undergoes a characteristic spectral shift in its emission depending on the polarity of its environment.[35]

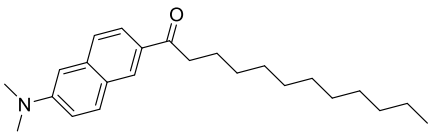

Figure 7. Structure of Laurdan, a naphthalene derivative used as a fluorescent membrane probe

Polarity-sensitive probes like Laurdan and some other naphthalene derivatives have been successfully used to study the environment in micelles, as well as natural and synthetic membranes.[35] The fluorescent naphthalene moiety in Laurdan has a dipole moment because of partial charge separation resulting from interaction of the electron-donating amino group and the electron-withdrawing carbonyl group.[37] Excitation increases the dipole moment, which will result in reorientation of solvent dipoles. In highly polar solvents like water, the excited state is significantly stabilized, resulting in a red shift in the emitted light, whereas in non-polar solvents,

there is little stabilization, resulting in a blue shift.[36] Parasassi et al.[36] reported results from the analysis of phospholipid vesicles in the gel and liquid crystalline states. The phase of the phospholipid molecule determines the emission maxima of Laurdan, green (~490 nm) in the fluid/liquid-crystalline phase and blueish (~440 nm) in the gel/ phase.[36] The overall fluidity of a membrane can be assessed by the relative intensities of the blue and green emissions (I_{440} and I_{490}, respectively) through the generalized polarization (GP) of Laurdan:

$$GP = \frac{I_{440} - I_{490}}{I_{440} + I_{490}} \qquad (1.1)$$

GP thus allows for quantitative characterization of the phase state of the bilayer.

Statement of Problem

Increasing global population results in higher demands for energy to improve the quality of life.[37] Fossil fuels have been the main source of energy for a long time, but this dependence has presented environmental issues from combustion as well as sustainability issues.[37,38] Biofuels are a promising and sustainable alternative to fossil fuels that could increase energy security and reduce vehicle emissions of gases that contribute to pollution and global warming.[39] The European Union since the Kyoto protocol has been leading research in the development, production and the use of biofuels as a renewable energy source. The United States, in its Energy Independence and Security Act of 2007, set a requirement to use at least 36 billion gallons of biofuel by 2022, with 21 billion gallons being derived from non-cornstarch products, including cellulosic biomass.[40,41]

Bio-alcohols specifically are important sources of transportation fuel to reduce carbon dioxide emissions. They are produced by microbial fermentation of feedstocks rich in carbohydrates, such as sugar, starch and cellulose. Several challenges emanate from biofuel production, which include:

1. The hygroscopicity and corrosivity of ethanol, making it incompatible with current fuel storage and distribution infrastructure.[40] Several billion dollars have been invested to improve infrastructure, but advanced biofuels that can directly substitute for hydrocarbons are also being developed.

2. Competition with land use for crops results in increased food costs.[38] A potential mitigation is to obtain biofuels from more abundant lignocellulosic biomass (made up of cellulose, hemicellulose and lignin).[38] However, this approach creates new challenges due to difficulty in the breakdown of cellulose and hemicellulose embedded in the insoluble, highly cross-linked polymer lignin. The crystalline microfibrils of cellulose make it difficult to access the simple sugar units for breakdown by microorganisms and further conversion into fuel. Extensive research in this area continues, for example investigations of novel enzymes like cellulases from protists that reside in the gut of termites that would help in the breakdown of these polymers.[42–44]

3. The disruptive effect of the biofuels and other organic solvents (used in conversion processes to help break down lignocellulosic biomass) on the membrane of the microbes used in the conversion process.[45,46] The toxicity of the products fermentation to the producer organism limits fuel titers and yields, making the overall process economically inviable. Despite research for decades into microbes capable of biofuel tolerance production, success remains illusory.[45,46] An approach under consideration and gaining some recognition is engineering microbial membranes for robustness to withstand solvent-induced stress.[46] The strategy is to study and understand the details of solvent-induced stress on the membrane, its integrity as a barrier, and its many functions, such as communication and transport.[46,47] One area of research focuses on membrane-bound

transporters, with the goal of boosting the secretion of biofuels.[48,49] For example, a family of wax transporters have been identified as a possible means of secreting ketones, long chain alkanes, alcohols, aldehydes, and possibly fatty acids from cells.[49–51] A challenge in this areas is the inability to define mechanisms involved in the process.

Research into engineering the fatty acid composition of the membrane to withstand fuel stress has also been on the rise. In that regard, the Standaert group aims to contribute by investigating the influence of membrane composition on resistance to fuels and solvent.

4. This research is driven in the direction to create membrane models for *Bacillus subtilis*, a harmless soil organism and candidate biofuel producer, and study their response to solvent stress.

Research Plan

This research focuses specifically on the synthesis of phosphatidylethanolamine, a phospholipid known to be abundant in the membrane of *B. subtilis*. Gram-positive bacteria such as *B. subtilis* use unusual branched, saturated fatty acids (iso- and anteiso-branched chains of 14 to 17 carbon atoms, Figure 8) in their membrane phospholipids. None of the phospholipids (Figure 9) are commercially available, and the fatty acids themselves are available only in small quantities at high cost.

In order to study fuel and solvent stress on bacterial membranes, we therefore established three primary objectives as the bases of this research.

1. Make phosphatidylethanolamine lipids with different combinations of unique fatty acids tails (Figure 8) that are found in the membrane of *Bacillus*.

2. Make vesicles of these lipids as models of the bacterial membrane and analyze membrane fluidity (using Laurdan) to understand the effect of stresses of varied types (temperature and solvent concentration) on cell membranes of microorganisms relevant to biofuel production.

3. Suggest possible stress-resistant cell membrane compositions for consideration in biofuel production.

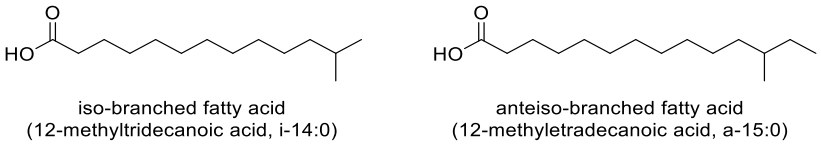

Figure 8. Branched fatty acid types found in *Bacillus*

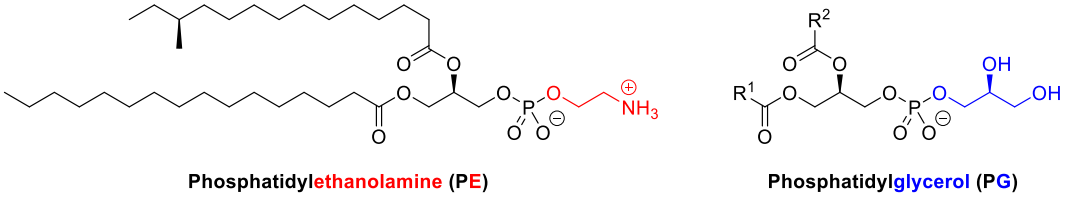

Figure 9. The structures of major phospholipids found in *Bacillus subtilis* cell membrane

CHAPTER 2. EXPERIMENTAL METHODS

Chemicals and Materials

The chemicals that were used for the synthesis and studies are: 11-bromoundecanoic acid, 12-hydroxydodecanoic acid, zinc powder, phosphorous oxychloride ($POCl_3$), various Grignard reagents (isobutyl magnesium chloride, isopropyl magnesium chloride, *sec*-butyl magnesium chloride lithium chloride complex, isopentyl magnesium bromide, and 2-methyl butyl magnesium chloride) purchased from Sigma Aldrich; dilithium tetrachlorocuprate (DTCC), di-*tert*-butyl *N*,*N*-diisopropylphosphoramidite, *meta*-chloroperbenzoic acid (MCPBA), chloroform, ether, *N*,*N*-dimethylformamide, 4-dimethylaminopyridine (DMAP), β,β,β-trichloroethyl choroformate, trichloroacetonitrile, chloroform-*d* ($CDCl_3$) and quinoline purchased from Acros Organics; cesium carbonate (Cs_2CO_3), 1*H*-tetrazole, triethylamine, thionyl chloride, Dowex 50 (H^+) ion-exchange resin, and tetrahydrofuran (THF) from Alfa Aesar; acetonitrile, chloroform hexane, methanol, dichloromethane, toluene, sulfuric acid, acetone, TFA, acetic acid, acetic anhydride, concentrated HCl and concentrated HBr purchased from Fisher Chemical; and diisopropylethylamine (DIPEA), dicylohexyl carbodiimide (DCC), (*S*)-glycidol, solketal (1,2-isopropylidene-s*n*-glycerol) purchased from TCI America; palmitic acid purchased from MP Biomedicals; and silica gel purchased from Silicycle.

NMR Analysis

All synthesized compounds were analyzed with a JEOL-NMR Eclipse 400-MHz spectrophotometer to verify the chemical structure and purity of the samples. Samples were freed from residual solvents by dissolution in and evaporation from chloroform, followed by chloroform-*d*, prior to final dissolution in chloroform-*d*.

Fatty Acid Analysis by GC–MS

Gas chromatography–mass spectrometry (GC–MS) was performed on a Shimadzu GC-2010 gas chromatograph equipped with an AOC-20i autosampler, an SHRXI-5MS capillary column (length 30 m, inside diameter 0.25 mm, film thickness 0.25 μm) and a GCMS-QP2010 mass-sensitive detector operating in electron impact mode at 70eV.

Analyses were performed using He carrier gas at a flow rate of 1 mL/min, an inlet temperature of 260 ℃, an ion-source temperature of 200 ℃, and a transfer line temperature of 250 ℃. The initial oven temperature of 50 ℃ was held for 2 min, ramped at 20 ℃/min to 280 ℃, and held for 2 min. An injection volume of 1 μL and a split ratio of 20:1 were used.

GC–MS analysis was conducted on the synthesized fatty acids both post-synthesis and during Grignard couplings with 11-bromoundecanoic acid to ensure that all the starting material was consumed during reactions. Fatty acids were analyzed as their corresponding fatty acid methyl esters (FAMEs) because fatty acids have a poor chromatographic behavior. A small portion (~100 μg) of fatty acid was dissolved in 1 mL of 10% concentrated HCl in methanol, and the solution was heated in a sealed test tube at 85 °C for 2 h. After cooling, water (1 mL) and hexane (1 mL) were added, the sample was vortex-mixed, and the phases were allowed to separate. The organic (top hexane) layer was carefully collected and diluted to 1 mL with hexane in a 2-mL autosampler vial.

Synthesis of 12-Bromododecanoic Acid

The approach of Lewis and Reber[52] was employed to synthesize 12-bromododecanoic acid from 12-hydroxydodecanoic acid (Figure 10).

12-Hydroxydodecanoic acid (4.0 g, 0.021 mol) was heated to reflux with stirring in 4.0 mL of 48% aqueous hydrobromic acid at 80 °C for 4 hours. An extra 4.0 mL of the 48% aqueous hydrobromic acid was added, reflux was resumed for a further 4 h. The reaction mixture was diluted with water, extracted into DCM (CH_2Cl_2) and dried over anhydrous sodium sulfate. The solvent was evaporated to give a crude yellowish oil which was recrystallized from hexane to give an off-white powder: ^{1}H NMR (400 MHz, $CDCl_3$) δ (ppm) 1.25 (br m, 12H), 1.40 (br p, 2H, *J*= 7.0 Hz), 1.61 (p, 2H, *J* = 7.3 Hz), 1.83 (p, 2H *J*= 7.2 Hz), 2.33 (t, 2H, *J* = 7.6 Hz), 3.39 (t, 2H, *J* = 7.0 Hz), 9.2 (br s, 1H).

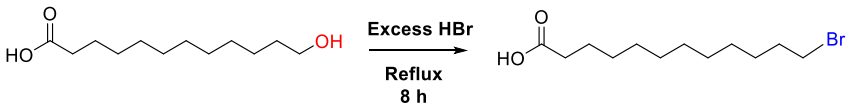

Figure 10. General scheme for the synthesis of an ω-bromo-acid

Synthesis of 13-Methyltetradecanoic Acid (i-15:0)

The approach of Baer and Carney[53] was employed for the synthesis of fatty acids from Grignard reagents and ω-bromoacids via a copper-catalyzed coupling (Figure 11).

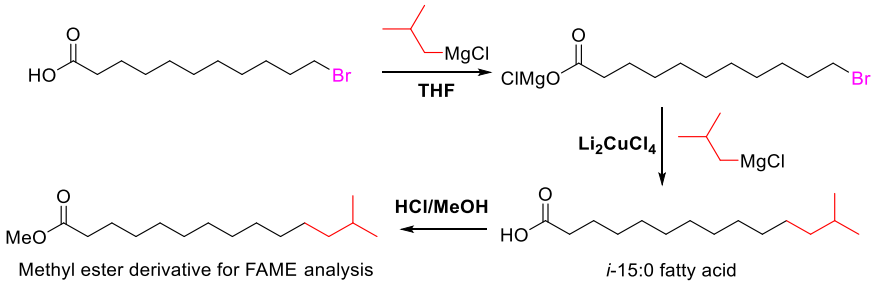

Figure 11. General scheme for the synthesis of fatty acids from a Grignard reagent and an ω-bromoacid

To a round bottom flask equipped with a stir bar was added 2.045 g (7.71 mmol) of 11-bromoundecanoic acid. The flask was sealed and flushed with nitrogen gas, after which anhydrous THF (9.4 mL) was added, and the solution cooled with stirring to −25 ºC (in an isopropanol bath cooled with dry ice). Isobutylmagnesium chloride (3.75 mL of a 2.0 M solution in THF, 7.5 mmol, 0.97 equiv) was added dropwise while the temperature was maintained. Diithium tetrachlorocuprate (1.5 mL of a 0.1 M solution in THF, 0.15 mmol, 0.02 equiv) added followed by an additional 4.0 mL (8.0 mmol) of the Grignard reagent were added dropwise while the bath temperature was maintained at −20 to −25 °C. The reaction flask was transferred into a freezer and kept at −20 °C overnight. A portion of the reaction (~1 μL) of the reaction mixture was withdrawn for FAME analysis (above). If unreacted 11-bromoundecanoic acid was detected, proportionate additions of DTCC and Grignard reagent were added as necessary, followed by additional reaction time, until repeate analysis showed that 11-bromoundecanoic acid had been completely consumed.

The reaction mixture was cautiously transferred with the aid of 50 mL of toluene into a separatory funnel containing 25 mL of 1 M H_2SO_4. After extraction and removal of the aqueous layer, the organic layer was washed with water containing 33 mg of sodium sulfide (~0.4 mmol) to precipitate residual copper salts. The organic layer was filtered, dried over sodium sulfate, and evaporated under reduced pressure. The crude acid was purified by bulb-to-bulb distillation under vacuum at an oven temperature of approximately 190–200 ºC using the apparatus depicted in Figure 12. The collected fatty acid was melted into a pre-weighed vial, affording 1.02 g (4.21 mmol, 55%) of the product as a white or off-white solid. ^{1}H NMR (400 MHz, $CDCl_3$) δ (ppm), 9.7 (br s, 1H), 2.33 (t, 2H, J = 7.5 Hz), 1.62 (p, 2H, J = 7.3 Hz), 1.50 (sept, 1H, J = 6.6 Hz), 1.24-1.31 (m, 16H), 1.13 (br q, 2H, J = 6.8 Hz) and 0.85 (d, 6H, J = 6.6 Hz). Examination of the

^{1}H NMR spectrum revealed minor impurities with resonances at δ 0.9 and 3–5 ppm (Appendix). Following Baer and Carney, the product was dissolved in hexane (10 mL) washed with water, filtered and crystallized, resulting in substantial reduction of the impurity peaks.

Figure 12. Apparatus for bulb-to-bulb vacuum distillation

Unilamelar Vesicle Preparation and Laurdan Fluidity Analysis

1-Palmitoyl-2-oleoyl phosphatidylethanolamine (POPE) and 1-Stearoyl-2-oleoyl phosphatidylglycerol (SOPG) vesicles were prepared in a 3:1 (POPE/SOPG) mole ratio, doped with 0.5 mol % Laurdan. Thus, POPE and SOPG (10 mg/mL in chloroform) were mixed in proportions of 0.365 mL (3.65 mg, 5.08 μmol) and 0.135 mL (1.35 mg, 1.69 μmol), respectively, in an amber glass dram vial. Laurdan (0.34 mL of a 93-μM stock solution in methanol, 31.6 nmol) was added, and the solvents were evaporated under a stream of nitrogen. The residue was re-dissolved in chloroform and evaporated again to remove residual methanol, then dried overnight in a vacuum desiccator to obtain a dry film.

The lipids were hydrated by addition of 1 mL of water vortex mixing, and heating in water bath at 50 °C, producing a cloudy suspension. The suspension was subjected to five freeze/thaw cycles by freezing on dry ice/ethanol and thawing in the water bath (50 °C, 2 min with intermittent vortex mixing) to break down multilamellar vesicles. Small unilamellar vesicles 100 nm in diameter were prepared by extrusion of the suspension 31 times through 100 nm pore size polycarbonate membrane at 40–50 °C using an Avanti® mini extruder. The extruded vesicle suspension was kept in the dark until analysis after dilution to working concentrations of 0.5–1.0 mg/mL.

Fluorescence spectra were acquired using a Horiba FluoroMax-3, spectrometer with an excitation wavelength of 364 nm, excitation slit width of 0.25 nm, and emission slit width of 2 nm. Emission spectra were acquired over the range 401–471 nm with an increment of 2 nm. Temperature was controlled with a circulating bath, and sample temperatures were recorded using a digital thermometer. GP was calculated according to Eq. 1.1 using the fluorescence intensities at 439 and 489 nm.

Synthesis of the Glycerophosphate Backbone

(*R)-Di-O-tert-butylphosphorylglycidol (****1)***

A modification of the approach of Lindberg[54] and coworkers was employed. To a round bottom flask charged with (*S*)-glycidol (238 mg, 3.21 mmol) was added with stirring di-*tert*-butyl *N*,*N*-diisopropyl phosphoramidite (1.80 mL 1.58 g, 5.70 mmol, 1.78 equiv) and then 100 mL of DCM. 1H-Tetrazole (24 mL of a 0.45 M solution in acetonitrile, 10.8 mmol, 3.4 equiv) was added dropwise via syringe. After 30 min, the reaction vessel was placed into an ice bath, *m*-CPBA (70-75% purity, 1.70 g, ~6.9 mmol, ~1.2 equiv with respect to phosphoramidite) was added, and the solution was stirred for 40 minutes to oxidize the intermediate phosphite ester into

the phosphate ester, **1**. The contents of the flask were carefully transferred into a separatory funnel, extracted with about 40 mL of 10% aqueous $Na_2S_2O_3$ followed by saturated $NaHCO_3$, then dried over sodium sulfate, concentrated by rotary evaporation, and stored at −20 °C. Purification was performed by flash chromatography on silica gel with the apparatus depicted in Figure 13 using a step gradient of ethyl acetate:hexane in proportions of 2:1, 1:1 and finally 1:1.5, in all cases with 1% triethylamine to preserve the acid-labile *tert*-butyl phosphoesters. Evaporation of solvent from the product-containing fractions afforded 165 mg (17%) of the product as a colorless pale-yellow oil. ^{1}H NMR data matched those reported by Lindberg et al.

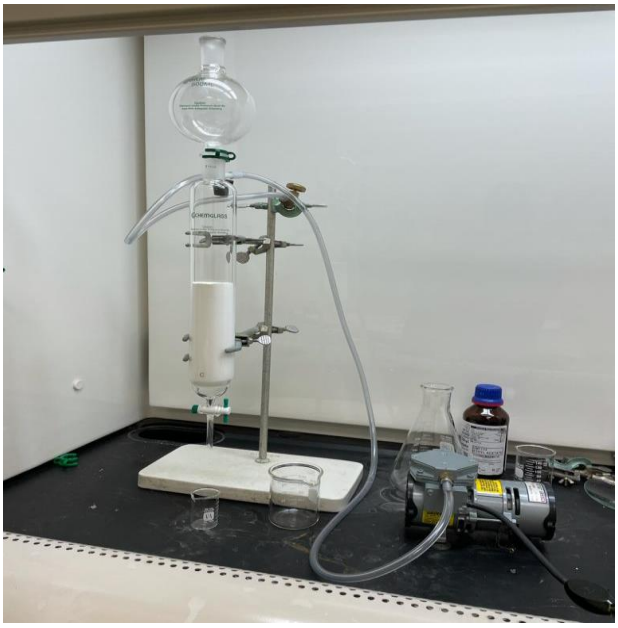

Figure 13. Apparatus for flash chromatography

Synthesis of cesium palmitate

Cesium palmitate was necessary to achieve a regioselective opening of the epoxide of compound **1**, as depicted in Figure 14.

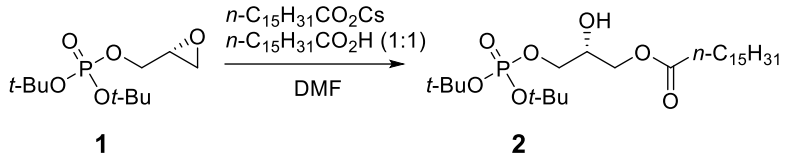

Figure 14. A synthetic pathway for the regiospecific epoxide opening

The synthesis of cesium palmitate was carried out with a procedure adopted from Kruinzinga and coworkers.[55] Cesium carbonate (325 mg, 1 mmol) in 10 mL of methanol was warmed to about 40 °C. Palmitic acid (770 mg, 3 mmol, 1.5 equiv) was added in portions while stirring for 30 min. After the mixture was cooled to room temperature, the product was precipitated with 50 mL of ether, collected by filtration, and washed extensively with ether to remove excess palmitic acid. The residue was dried in vacuo, to yield 521 mg (1.34 mmol, 67%) of cesium palmitate.

CHAPTER 3. RESULTS AND DISCUSSION

The Standaert research group is developing phospholipid models of the *Bacillus subtilis* cell membrane with branched fatty acids and employing fluorescence techniques with Laurdan general polarization to study fluidity of the models. Toward these goals, I concentrated on synthesizing model bacterial phosphatidylethanolamine (PE) lipids such as **6**, (Figure 15). The fatty acids indicated in Figure 15, 16:0 and i-15:0, are common in *B. subtilis* lipids, but other combinations will need to be made. My colleagues in the group targeted phosphatidylglycerol (PG) and phosphatidylcholine (PC) lipids which are chimeras employing bacterial fatty acids with a mammalian lipid head group, phosphocholine.

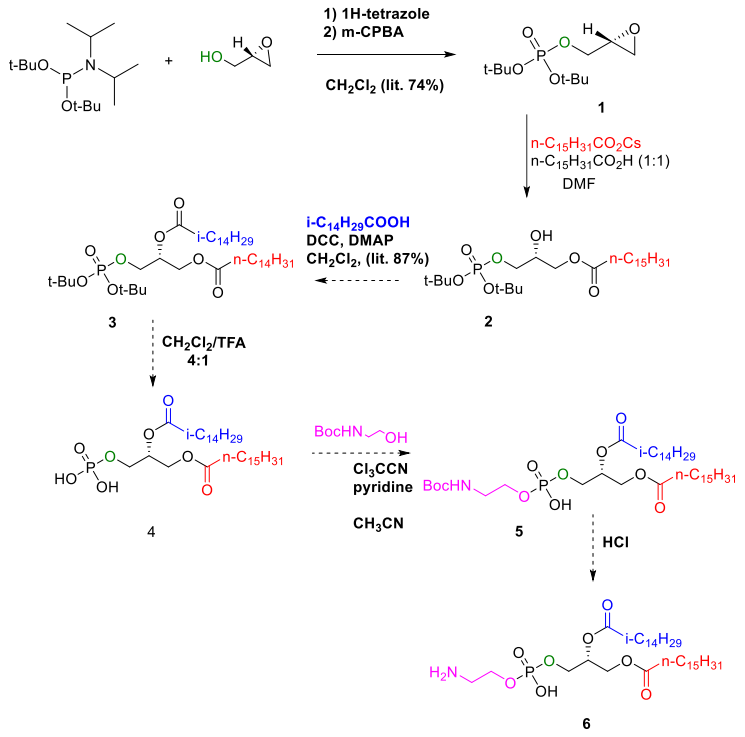

Figure 15. Synthetic route for bacterial phosphatidylethanolamine lipids. Solid arrows denote completed steps, whereas dashed arrows denote planned steps

To make **6**, commercial (*S*)-glycidol was converted to protected phosphate ester **1**, (*R*)-di-*tert*-butyl-phosphorylglycidol, by phosphorylation using phosphoramidite chemistry followed by *in-situ* oxidation to the phosphate (Figure 16). Epoxide **1** will undergo a regioselective S_N2 nucleophilic opening with cesium palmitate and palmitic acid to give **2**, 3-*O*-di-*tert*-butylphosphoryl-2-*O*-palmitoyl-*sn*-glycerol. Esterification of **2** with 13-methyl tetradecanoic acid (*i*-15:0) will produce the di-*tert*butyl protected phosphatidic acid **3**. Treatment of **3** with TFA in CH_2Cl_2 will afford the deprotected phosphatidic acid, **4**. Installation of the ethanolamine moiety will be accomplished by phosphoesterification with Boc-protected ethanolamine using trichloroacetonitrile as the reagent, followed by removal of the Boc group with acid to give **6**.

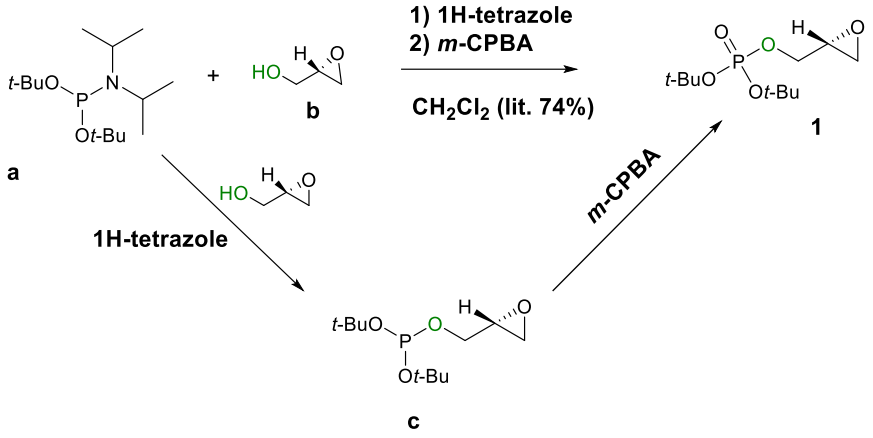

Figure 16. Scheme for the synthesis of the phosphate ester. Adapted from Lindberg and co-workers, 2002[48]

Synthesis of 12-Bromododecanoic Acid

As a group, we were able to make a total of five different iso and ante-iso branched fatty acids (14 to 16 carbon chains) from 11-bromoundecanoic acid, with my contribution being 13-methyltetradecanoic acid, and characterize them using GC–MS and ^{1}H NMR.

To make longer, C_{17} fatty acids used commonly by *B. subtilis* using readily available Grignard reagents, we require 12-bromododecanoic acid. In an initial attempt, we treated 12-hydroxydodecanoic acid with H_2SO_4 and HBr.[56] This method gave a low yield (32%), and the reaction was messy and difficult to work up. As a result, another procedure was employed (Figure 10) using excess HBr and 12-hydroxy acid only.[52] This method afforded a much higher yield of 78%, a cleaner reaction mixture and a simpler workup.

Figure 17. Two batches of 12-bromododecanoic acid synthesized from 12-hydroxy acid via two different procedures

Analysis of the 12-bromododecanoic acid as its FAME derivative showed the expected product at a retention time of 11.90 min (Figure 18). In the mass spectrum (Figure 19), a weak molecular ion was observed, with peaks of equal intensity at *m/z* 292 and 294 reflecting the equal abundance of ^{79}Br and ^{81}Br, along with expected fragments at 261/263 (loss of methoxy) and 213 (loss of Br). A significant impurity peak representing approximately 35% of the product was observed at a shorter retention time of 11.43 min. The mass spectrum of this compound was very similar to that of the expected product but lacked the molecular ion. Close examination of the mass spectrum led to the identification of this impurity as 12-chlorododecanoic acid, produced as an artifact of derivatization caused by substitution of bromide by chloride from the methanolic

HCl used in FAME derivatization. The mass spectrum similarly displayed a weak molecular ion peak at m/z 248 and 250, with intensities in the characteristic 3:1 ratio of ^{35}Cl to ^{37}Cl, and analogous fragment ions at 217/219 (loss of methoxy) and 213 (loss of Cl). The mass spectra of 12-chloro- and 12-bromododecanoic acids (Figure 19) and the ^{1}H NMR spectrum of 12-bromododecanoic acid (Figure 20) are given below.

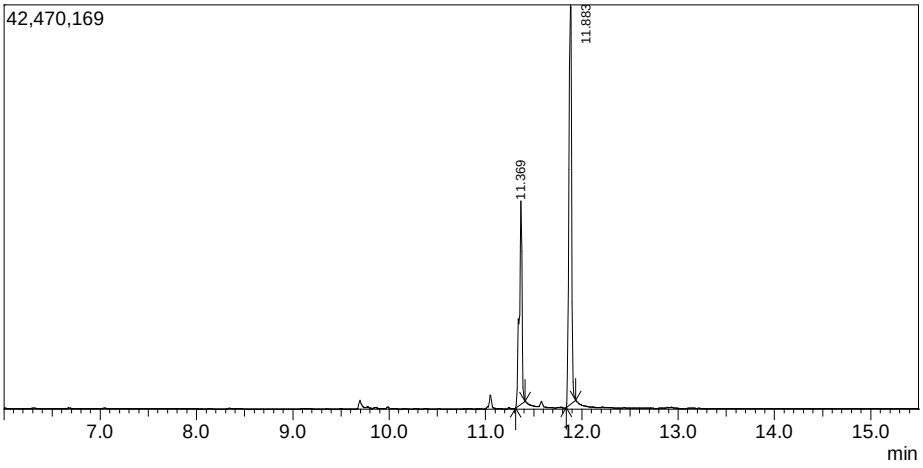

Peak Report TIC

Peak#	R.Time	I.Time	F.Time	Area	Area%	Height	Height%	A/H
1	11.369	11.313	11.411	41273183	32.59	21326141	33.72	1.94
2	11.883	11.838	11.936	85388124	67.41	41924385	66.28	2.04
				126661307	100.00	63250526	100.00	

Figure 18. Total ion gas chromatogram of 12-bromododecanoic acid methyl ester

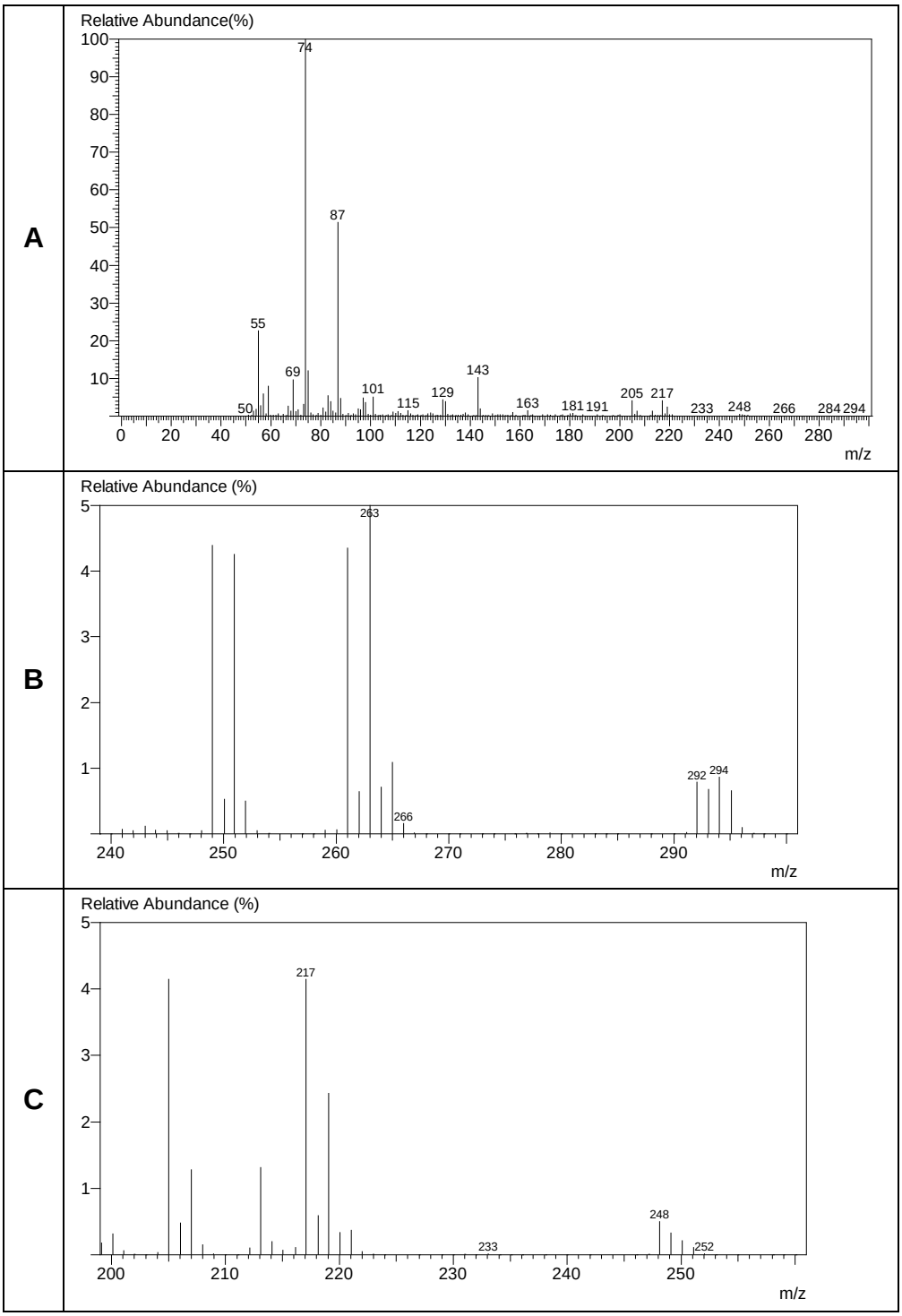

Figure 19. Electron-impact mass spectra of 12-bromo- and 12-chlorododecanoic acid methyl esters. (A) and (B) Full spectrum and molecular ion region, respectively, of 12-bromododecanoic acid methyl ester (t_R = 11.883 min, Figure 17) showing M+ (*m/z* 292 and 294) and M−OCH_3 (261 and 263); (C) Molecular ion region of 12-chlorododecanoic methyl ester (t_R = 11.389 min) showing M+ (*m/z* 248 and 250), M−OCH_3 (217 and 219) and M−Cl (213)

The ^{1}H NMR spectrum of the bromoacid revealed all the expected resonances and was consistent with the literature.[57] Two unexpected resonances, a triplet at δ 4.04 and a singlet at δ 2.04 were noted, indicating minor impurities. The latter might be a trace of acetone. The former is unassigned but could potentially be removed by recrystallization.

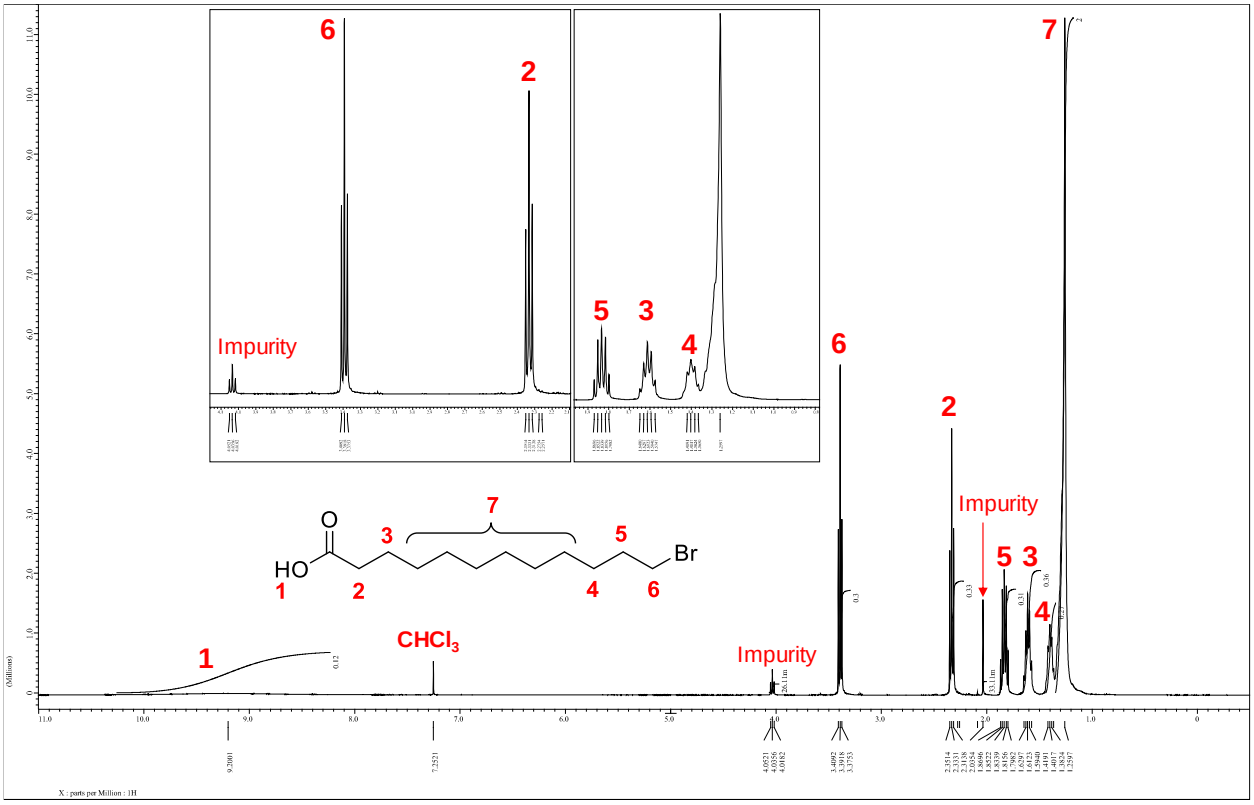

Figure 20. ^{1}H NMR spectrum of 12-bromododecanoic acid

Synthesis of Fatty Acids

One major aspect of this work is to make the various branched fatty acids that are not commercially available at reasonable cost. These fatty acids have 14- to 17-carbon chains with the two unique types of branching, iso- and anteiso-, which are found in the fatty acids in the cell membrane of *Bacillus subtilis.*

In my work, I prepared 13-methyltetradecanoic acid (i-15:0) using a copper-catalyzed Grignard coupling of 11-bromoundecanoic acid and isopropyl magnesium chloride. Baer and Carney[53] developed this approach and reported yields from 40% to 94% upon treating various Grignard reagents with different ω-bromoacids. In two replicate syntheses of i-15:0, I obtained yields of 55% and 47% (Table 1). These yields were consistent with Baer and Carney's precedent but not at the high end. Some losses could be associated with extraction and the purification steps.

The synthesized fatty acid was purified through bulb-to-bulb vacuum distillation at an oven temperature of ~190 to 200 °C, affording the product as a whitish solid.

Table 1. Reagents and Yields for Syntheses of 13-Methyltetradecanoic Acid

Grignard Reagent	**11-Bromoundecanoic Acid (g)**	**Product**	**Yield (g)**	**Yield (%)**
Isobutyl magnesium chloride	2.036	13-methyltetradecanoic acid	1.02	55
Isobutyl magnesium chloride (2^{nd} synthesis)	2.045	13-methyltetradecanoic acid	0.87	47

Instrumental Analysis of Fatty Acids

The synthetic i-15:0 was identified on the basis of its mass and ^{1}H NMR spectra. The gas chromatography (GC) total ion chromatogram of the product as its methyl ester (Figure 21) showed a single major peak at a retention time of 11.273 minutes. The mass spectrum of this compound (Figure 22) showed the expected molecular ion at m/z 256, along with a base peak at m/z 74 ($CH_3OC(OH)C=CH_2$) from the McLafferty rearrangement characteristic of methyl esters.

Additional expected fragments at *m/z* 241 ($M-CH_3$), 225 ($M-OCH_3$), and 213 ($M-C_3H_7$) were observed.

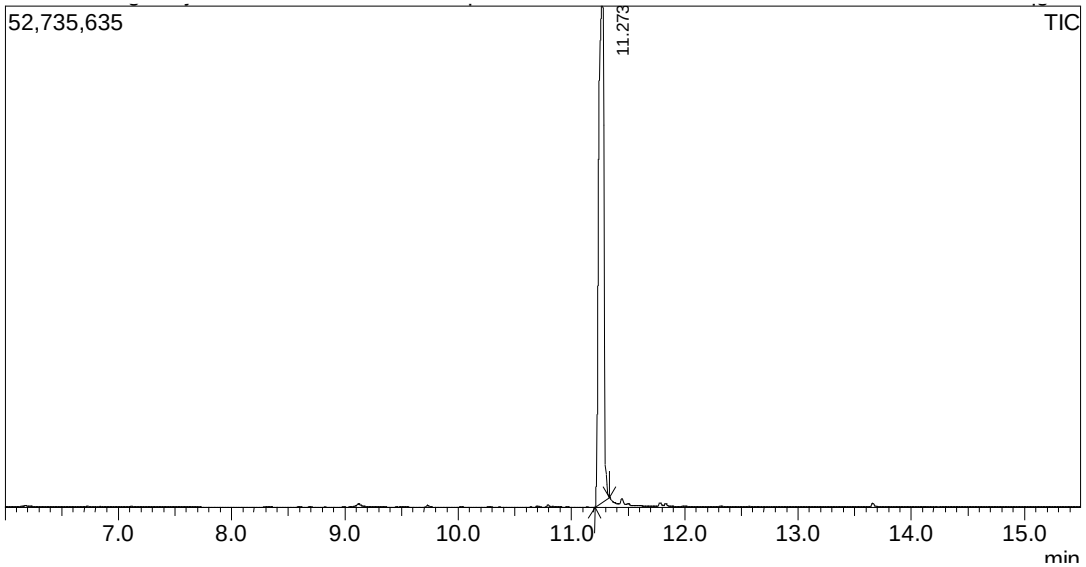

Peak Report TIC

Peak#	R.Time	I.Time	F.Time	Area	Area%	Height	Height%
1	11.273	11.208	11.334	161401511	100.00	52154531	100.00
				161401511	100.00	52154531	100.00

Figure 21. GC–MS total ion chromatogram of i-15:0 methyl ester

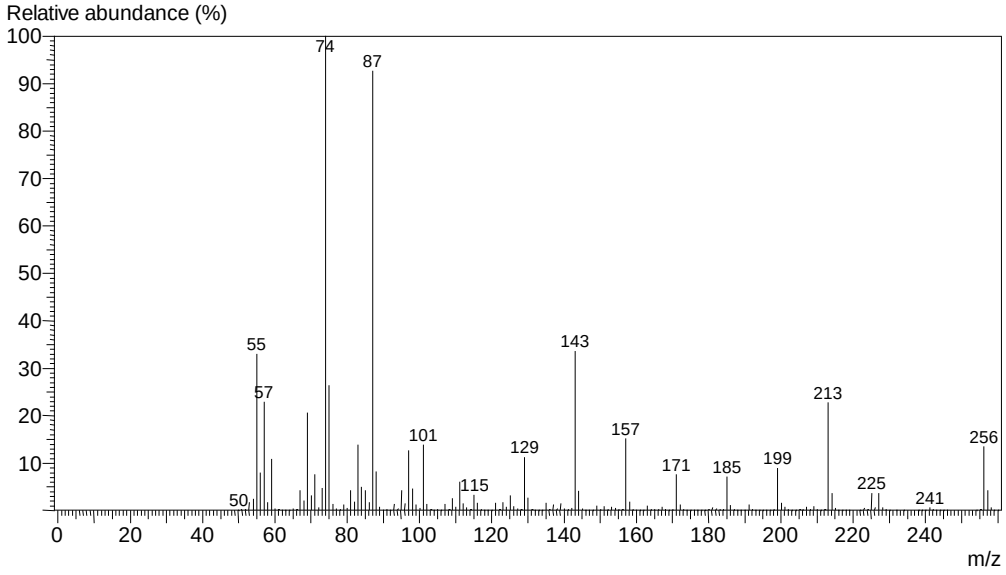

Figure 22. Electron-impact mass spectrum of i-15:0 methyl ester The molecular ion M+ is evident at *m/z* 256, along with the characteristic fragments $M-CH_3$ (241), $M-OCH_3$ (225),

M−C_3H_7 (213) and $CH_3OC(OH)C{=}CH_2$ (74). The spectrum shown is from t_R = 11.273 in Figure 20

GC–MS proved an important analytical tool for monitoring the progress of the coupling reaction. After every addition of the Grignard reagent, a small aliquot of the reaction mixture was subjected to FAME analysis to ascertain the presence of product and unreacted bromoacid in the vessel. Methyl esters have been a convenient way to analyze long-chain fatty acids because they have higher volatility and better chromatographic behavior than the parent acids.[58] The methyl esters of i-15:0 and 11-bromoundecanoic acid were well resolved by GC, with characteristic retention times of 11.28 and11.35 minutes, respectively (Figure 25). The bromoacid derivative was readily identified by analysis of the starting material. Reaction progress was monitored, and further additions of Grignard reagent were made until all the bromoacid was converted into product, as in Figure 21.

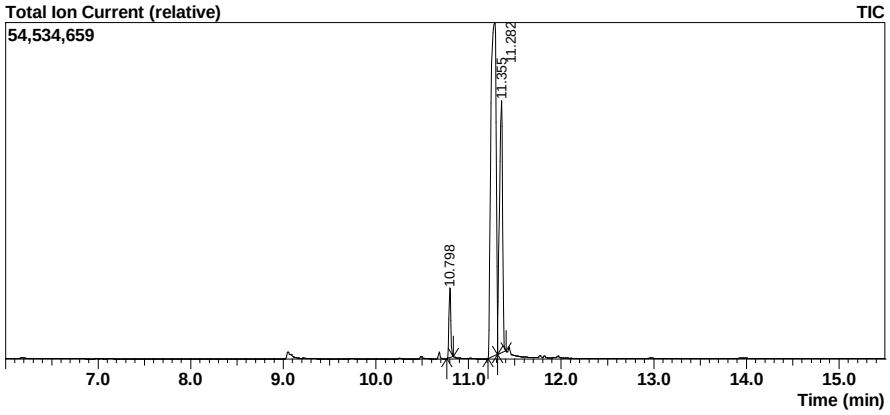

Peak Report TIC

Peak#	R.Time	I.Time	F.Time	Area	Area%	Height	Height%	A/H
1	10.798	10.767	10.837	16635809	5.11	11343787	10.69	1.47
2	11.282	11.208	11.313	215308442	66.07	53971471	50.84	3.99
3	11.355	11.313	11.404	93919124	28.82	40850243	38.48	2.30
				325863375	100.00	106165501	100.00	

Figure 23. GC–MS total ion chromatogram of i-15:0 methyl ester indicating an incomplete coupling reaction. The product is evident at t_R = 11.208 min, but significant amounts of the starting bromoacid (as its methyl ester) are evidenced by the peak at t_R = 11.355 min

To confirm the structure as well as the purity of the fatty acid, a ^{1}H NMR spectrum was recorded (full spectrum, Figure 24, and upfield expansion, Figure 25) The spectrum matched a literature report[59] and displayed all expected signals and multiplicities, with only trace impurities. Both the quantity and the quality of the material were sufficient for the synthesis of the targeted PE lipids.

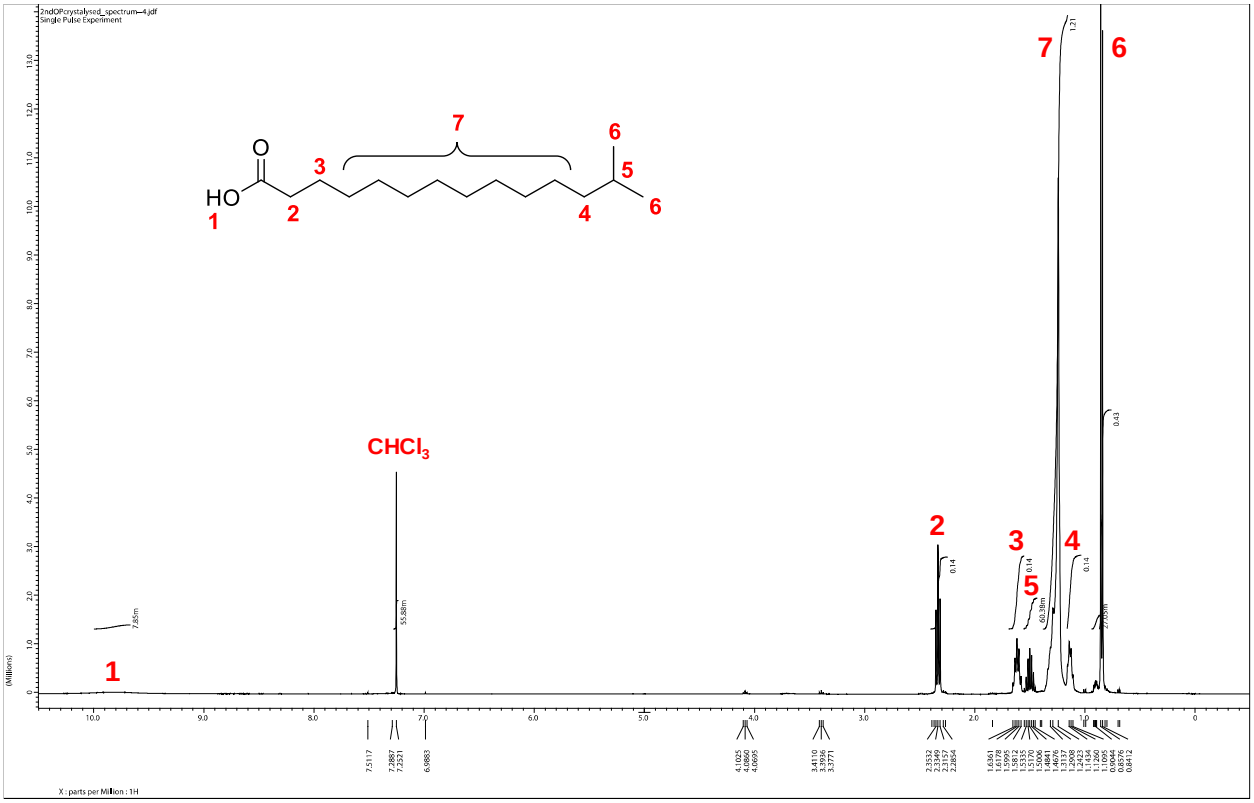

Figure 24. ^{1}H NMR spectrum of 13-methyl-tetradecanoic acid

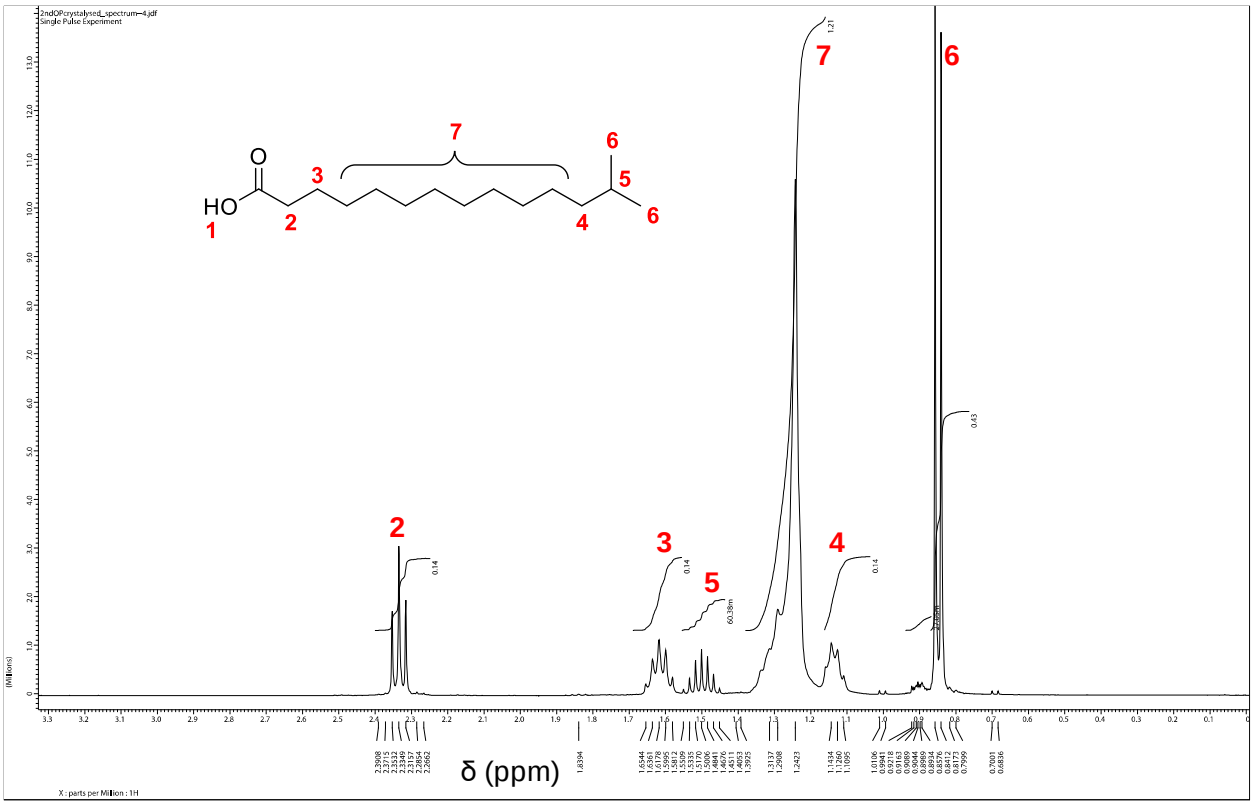

Figure 25. Upfield ^{1}H NMR spectrum of 13-methyl-tetradecanoic acid

Synthesis of (R)-Di-O-tert-Butylphosphorylglycidol

To make the phosphate head group for attachment with the fatty acids in making our phosphatidyl glycerol molecule, the reaction scheme presented in Figure 14 was followed to make the (*R*)-di-tert-butyl-phosphorylglycidol precursor. Flash chromatography with hexane:ethyl acetate; 2:1, 1:1, and finally 1:1.5 containing 0.1% triethylamine (NEt_3), was carried out to obtain the pure compound in a quantity of 165 mg and a yield of 17%. ^{1}H NMR analysis was employed to confirm that the correct product was isolated, with chemical shifts, integrals and multiplicities consistent with the literature.[54]

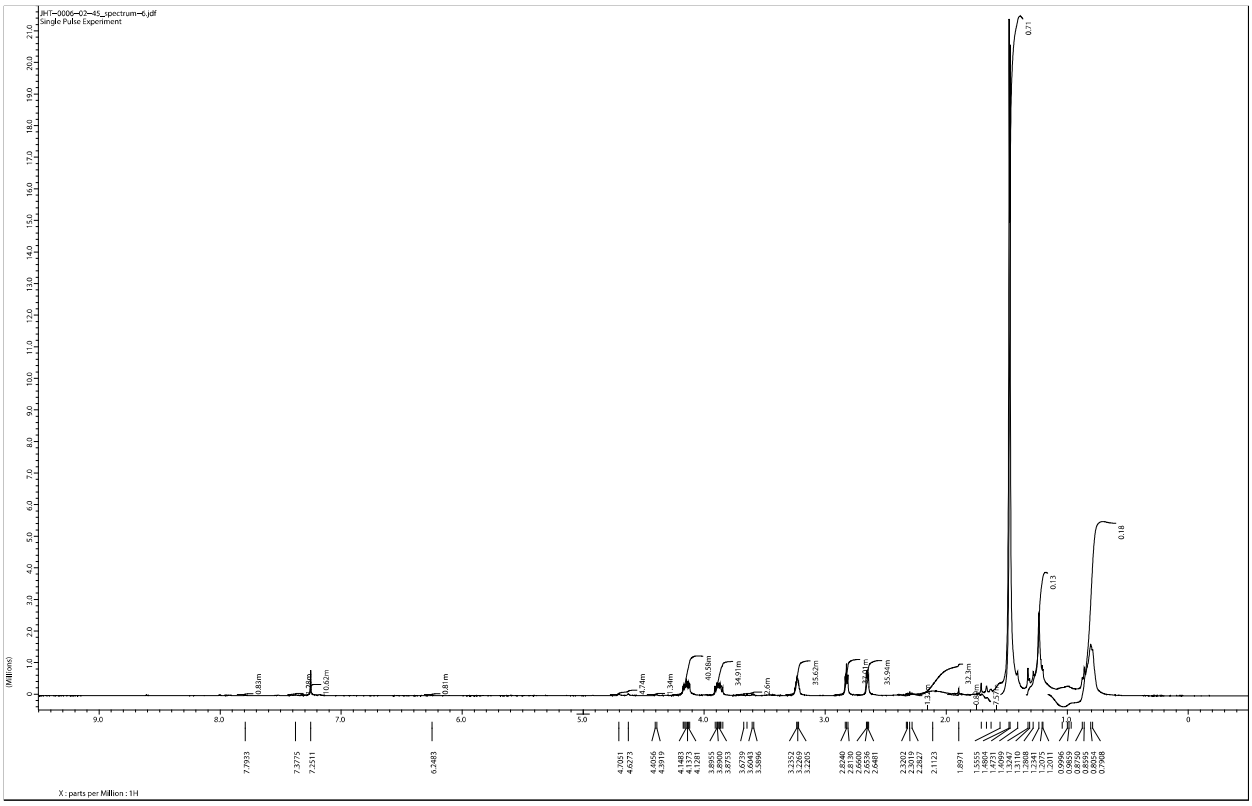

Figure 26. ^{1}H NMR for (*R*)-di-*O*-*tert*-butyl-phosphorylglycidol (**1**)

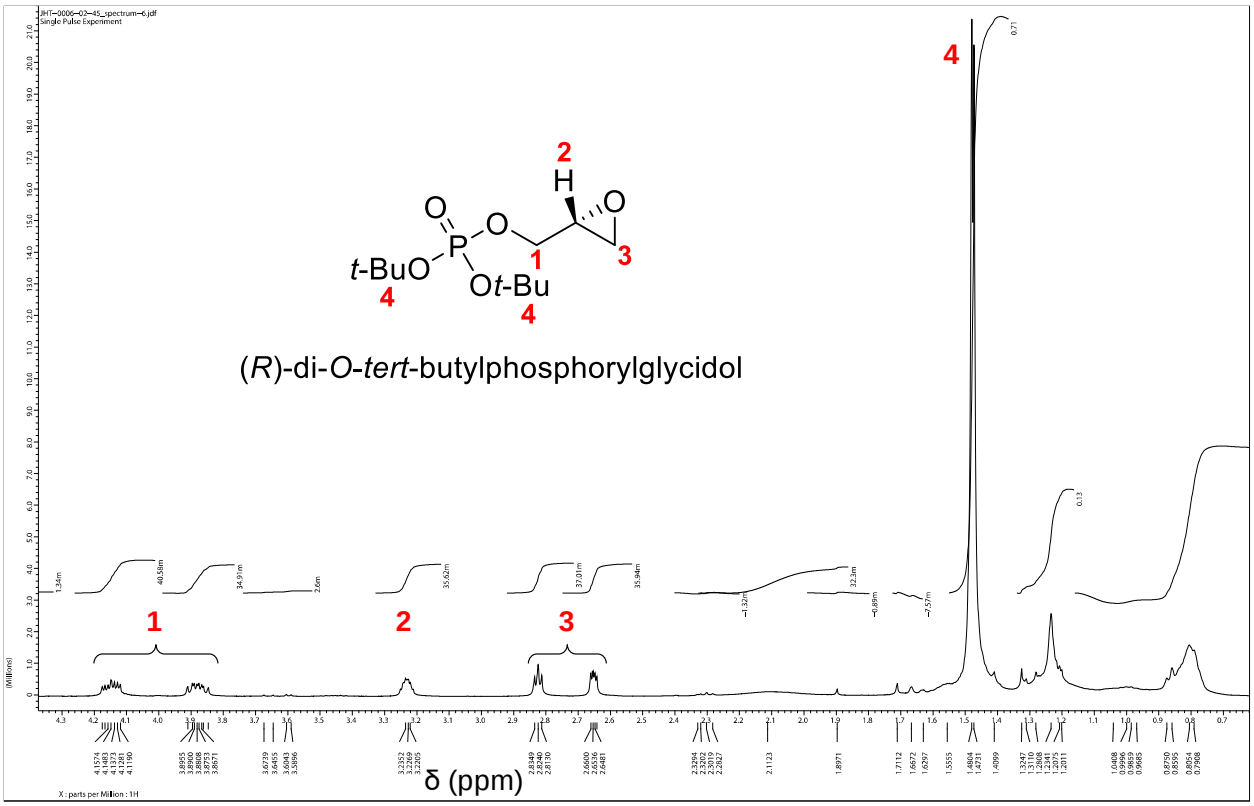

Figure 27. Upfield ^{1}H NMR for (*R*)-di-*O*-*tert*-butyl-phosphorylglycidol (**1**)

It was observed that a lot of the desired product was lost during the synthesis and purification. Since only the purest fractions were used, impure fractions that showed two spots with different retention factors, one for the desired product and another for any impurity, were not combined. Another reason to which low yield might be attributed was that the 1*H*-tetrazole used came in acetonitrile solution (instead of the solid that Lindberg and coworkers used). The large change in solvent polarity, or the undesired introduction of moisture present in the acetonitrile, could have adversely impacted the reaction by competing with glycidol for phosphorylation.

Synthesis of Cesium Palmitate and Epoxide Ring Opening

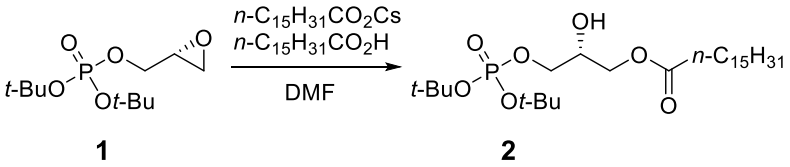

Figure 28. A synthetic pathway for protected lysophosphatidic acid via regiospecific epoxide opening

The synthesis of cesium palmitate was necessary to make a salt of our desired fatty acid, palmitic acid needed to achieve a regioselective opening of the epoxide of compound **4**, (*R*)-di-*tert*-butyl-phosphorylglycidol to achieve compound **5**, 3-*O*-di-*tert*-butylphosphoryl-2-*O*-palmitoyl-*sn*-glycerol. The synthesis of the cesium palmitate was successful with a 67% yield of a white powder that had a soapy appearance. The regiospecific epoxide ring opening of **4**, to produce **5,** was achieved on pilot scale only.

Determination of Membrane Polarity with Laurdan

While in the process of synthesizing our model phospholipids, we performed pilot fluidity experiments with commercially available mammalian lipids, 1-palmitoyl-2-oleoylphosphatidylethanolamine (POPE) and 1-stearoyl-2-oleoylphosphatidylglycerol (SOPG), as models of the bacterial membrane. These experiments were to validate the approach and help us understand the effect of fuels (and organic solvents) on the properties of the cell membrane. After making 100 nm unilamellar vesicles from 75:25 POPG:SOPG (mimicking the bacterial *B. subtilis* membrane composition) doped with 0.5 mole % Laurdan, membrane fluidity was monitored as a function of temperature and fuel (1-butanol) concentrations using Laurdan GP.

First, we examined temperature effects. Fluorescence emission spectra were recorded at temperatures from 20 ℃ to ~50 ℃ (Figure 29). These spectra displayed varying amounts of the

characteristic peaks at ~440 and ~490 nm expected of Laurdan in ordered and disordered environments, respectively. The 20 °C spectrum showed a predominant peak at the shorter wavelength and no peak at the longer wavelength, consistent with a highly ordered environment, possibly the gel phase. Raising the temperature produced an initially sharp reduction in the 440 nm peak, accompanied by growth of a perceptible 490 nm peak at 40 °C, marking a change from an ordered phase to a more disordered phase. Parasassi[36] and coworkers asserted that there is no temperature-dependent emission maximum shift in the gel or less fluid state of the phospholipids, but that there is a continuous shift above the gel→liquid crystalline transition temperature. Thus, our observations are consistent with the fluid phase at temperatures above 20 °C. The lack of a 490 nm peak at 20 °C, and the sharp decrease in the 440 nm peak above 20 °C, suggest a phase transition from gel to liquid crystalline near 20 °C. Increasing temperature further increased the red shift,[60] and at the highest temperature of 69 °C, the 440 nm peak was almost imperceptible, while the 490 nm peak was predominant. This shift of emission maxima is consistent with the expected progressive increase in fluidity and decrease in order.[60] In a highly ordered environment such as the gel phase, Laurdan is shielded from solvent, and only the 440 nm emission is observed. On the other hand, when the temperature increases the bilayer transitions to the liquid crystalline phase. As temperature is increased further, water penetration into the bilayer increases, resulting in the continuous red shift until only the 490 nm emission is observed. These changes can be quantified via GP of the Laurdan emission, as described in Eq 1.1 and presented below in Figure 30. Ordered environments have higher GP, while disordered ones have lower GP.

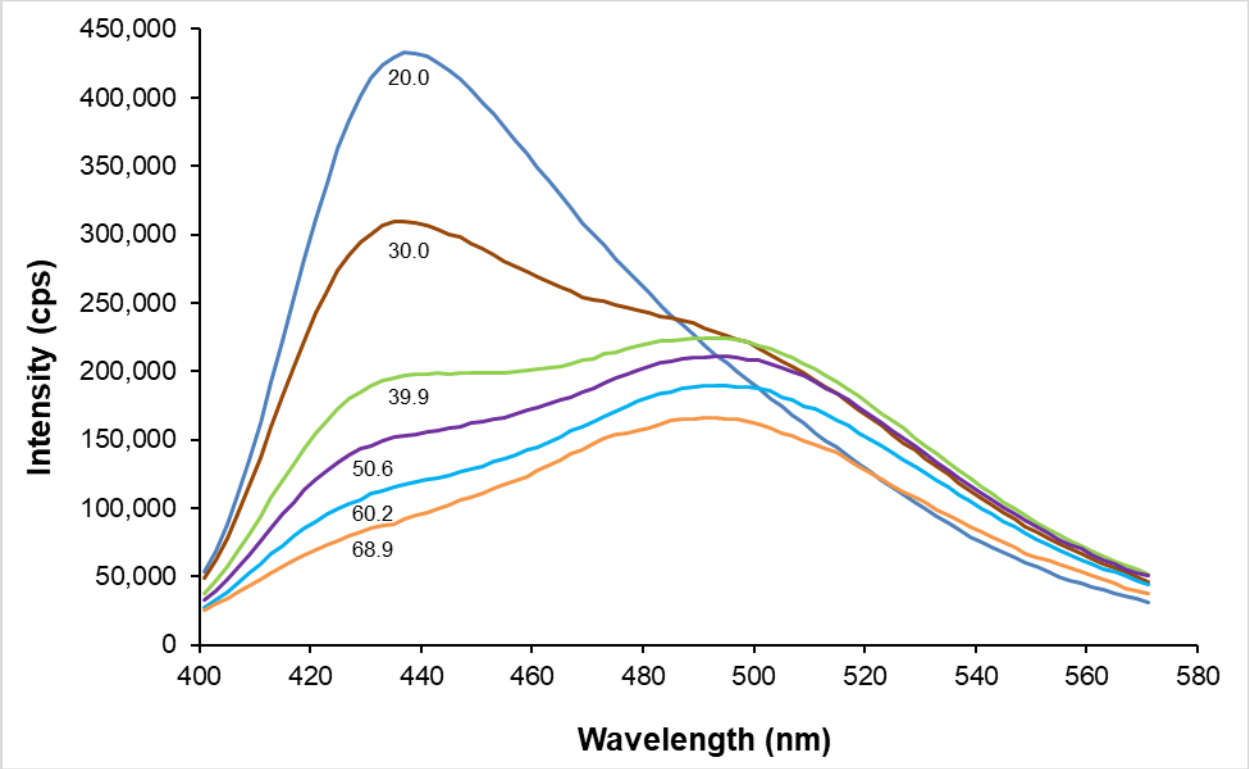

Figure 29. Effect of temperature on Laurdan emission spectra in POPE:SOPG (75:25) unilamellar vesicles. Increasing temperature increases fluidity and hydration, resulting in a progressive red shift in the emission spectrum

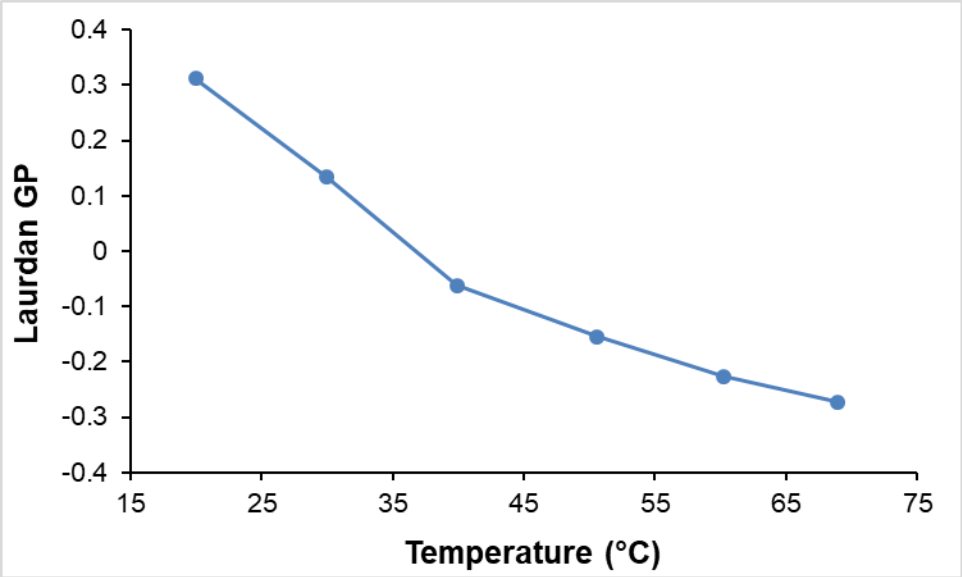

Figure 30. Laurdan GP in POPE:SOPG (75:25) vesicles as a function of temperature. Decreasing GP reflects increasing fluidity in the bilayer

We next examined Laurdan fluorescence as a function of 1-butanol concentrations from 0.1% to 3%. Addition of 0.1 or 0.3% 1-butanol had a negligible effect. Higher concentrations induced progressively stronger red shifts (Figure 31). These changes indicate that butanol increases fluidity and disordering, potentially inducing a gel → fluid transition at ~1% concentration. The transition temperature of the mixture studied has not been determined, but the highly ordered environment found at 20 °C (above) and the resistance to lower concentrations of butanol suggest the transition occurs near 20 °C. The overall fluidizing trend for 1-butanol concentration is similar to the result of heating and confirms the findings by Smith et al.[46] that 1-butanol has a potent fluidizing effect on membranes (Figure 32). Large changes in fluidity would require an adaptive response on the part of an organism producing 1-butanol by fermentation.

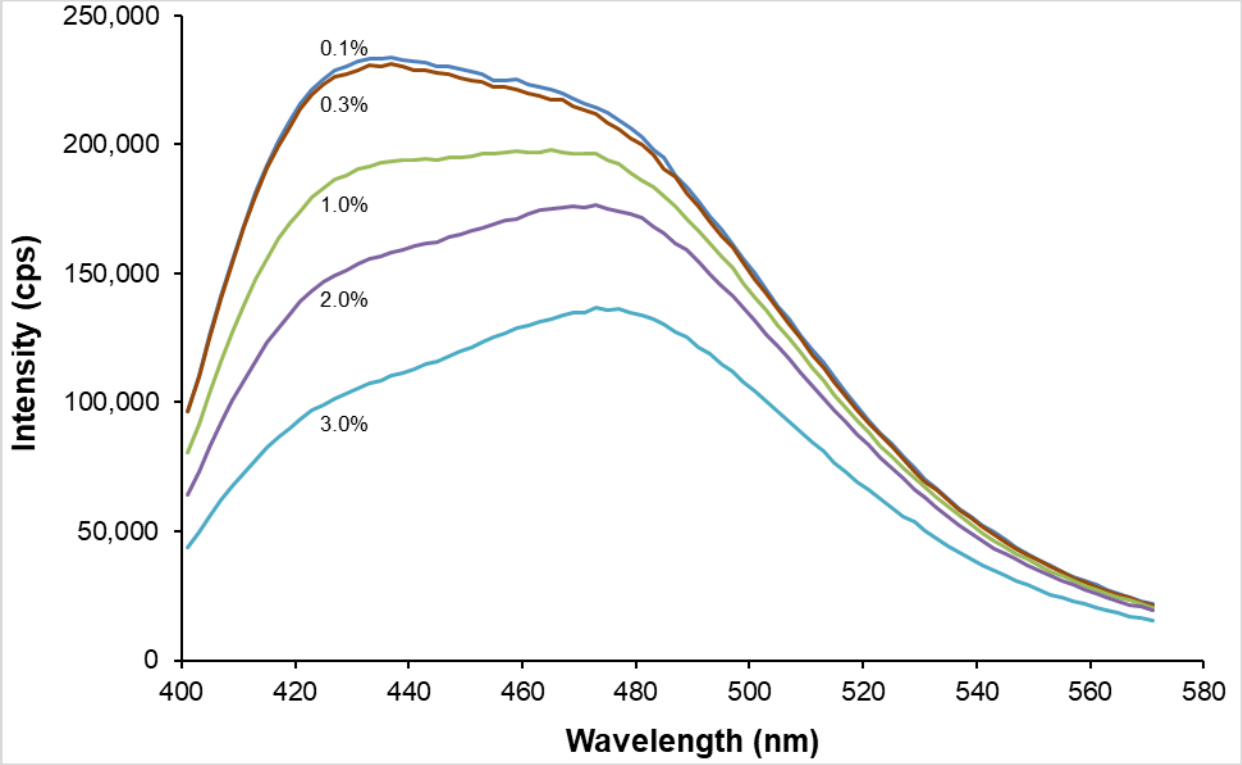

Figure 31. Effect of 1-butanol on Laurdan emission spectra in POPE:SOPG (75:25) unilamellar vesicles at 25 °C. Increasing 1-butanol concentration increases fluidity and hydration, resulting in a progressive red shift in the emission spectrum

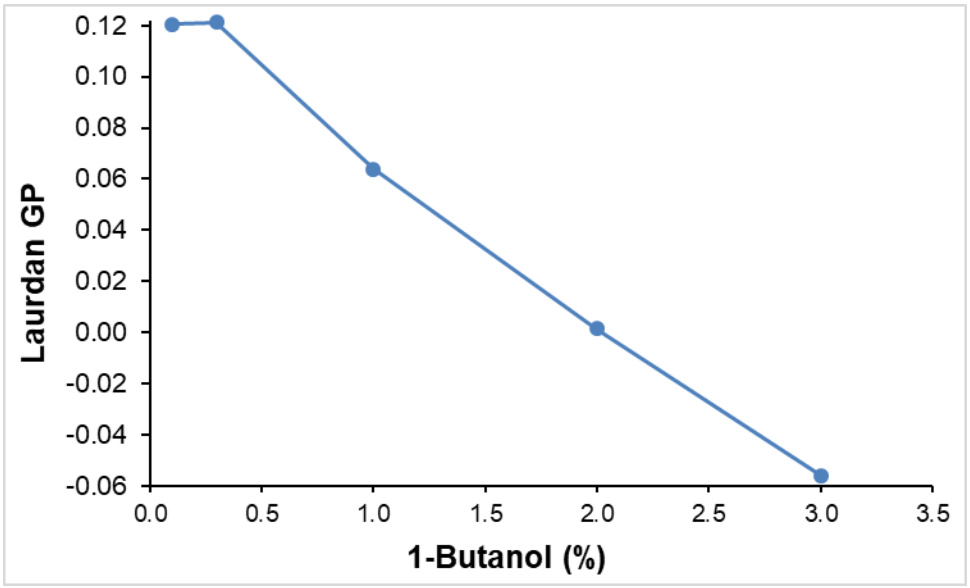

Figure 32. Laurdan GP in POPE:SOPG (75:25) vesicles as a function of 1-butanol concentration. Decreasing GP reflects increasing fluidity in the bilayer

CHAPTER 4. CONCLUSIONS AND FUTURE PROJECTIONS

The end goal of Dr. Standaert's research group is to make phospholipid models found in the membrane of *Bacillus subtilis* and use florescence techniques to study the interactions between the lipids under the various stress conditions associated with biofuel production, and their effects on microorganism cells. Toward this end, my work was directed at the synthesis of an important class of bacterial lipids, phosphatidylethanolamine (PE), the predominant component of bacterial plasma membranes. Colleagues in the laboratory focused on PG and PC lipids. The branched fatty acids for the bacterial lipids are not readily available, so I synthesized 13-Methyltetradecanoic acid (i-15:0) using a copper-catalyzed coupling of 11-bromoundecanoic acid with isopropylmagnesium chloride. Subsequently, I synthesized 12-bromododecanoic acid, a precursor to branched C_{17} fatty acids. Finally, I synthesized and purified (*R*)-di-*O-tert*-butylphosphorylglycidol (**1**), a key intermediate that will allow stereospecific and regioselective introduction of the *sn*-1 and *sn*-2 acyl groups and facilitate attachment of the head group. These compounds were all characterized by ^{1}H NMR analysis to confirm their identity and purity. 13-Methyltetradecanoic acid and 12-bromododecanoic acid were also characterized by GC–MS analysis. However, GC–MS was not a conclusive tool for structural analysis and purity determination, since ^{1}H NMR showed impurities in the products that were not detected by GC. Finally, I performed Laurdan GP studies on a model lipid mixture, POPE:SOPG (3:1) to demonstrate increasing fluidity in response to temperature and 1-butanol concentration. The success of these experiments validates the use of this approach for the study of membrane stress on the bacterial lipids.

However, due to delays from COVID-19 restrictions, we were unable to complete the syntheses of the target lipids. The next step (Figure 14) is regioselective opening of the epoxide

in **1** to install the *sn*-1 acyl chain. This reaction was performed on a pilot scale and appeared successful, but the product was not fully purified and characterized. A further coupling with the *sn*-2 fatty acid comes next, followed by coupling with the ethanolamine moiety to complete the synthesis of the phospholipid. Having these otherwise unavailable lipids will enable future studies on the effects of fuel and solvent stress via membrane fluidity analysis to further the economical production of sustainable biofuels.

REFERENCES

(1) Barák, I.; Muchová, K. The Role of Lipid Domains in Bacterial Cell Processes. *Int. J. Mol. Sci.* **2013**, *14* (2), 4050–4065. https://doi.org/10.3390/ijms14024050.

(2) Alvarez A.F., Georgellis D. Bacterial Lipid Domains and Their Role in Cell Processes. In *Geiger O,* (eds); Biogenesis of Fatty Acids, Lipids and Membranes. Handbook of Hydrocarbon and Lipid Microbiology. Springer, Cham., 2019; pp 575–592. https://doi.org/10.1007/978-3-319-50430-8_39.

(3) Lin, T. Y.; Weibel, D. B. Organization and Function of Anionic Phospholipids in Bacteria. *Appl. Microbiol. Biotechnol.* **2016**, *100* (10), 4255–4267. https://doi.org/10.1007/s00253-016-7468-x.

(4) Rossy, J.; Ma, Y.; Gaus, K. The Organisation of the Cell Membrane: Do Proteins Rule Lipids? *Curr. Opin. Chem. Biol.* **2014**, *20*, 54–59. https://doi.org/10.1016/j.cbpa.2014.04.009.

(5) Lehr, A.; Frank, A.; Münch, W.; Dietz, U.; Nubbemeyer, U. Synthesis of 1-Palmitoyl-2-*(E)*-9- and *(E)*-10-Nitrooleoyl)-*sn*-Glycero-3-Phosphatidylcholines. *Synthesis.* **2019**, *51* (17), 3295–3304. https://doi.org/10.1055/s-0037-1611530.

(6) Heberle, F. A.; Pan, J.; Standaert, R. F.; Drazba, P.; Kučerka, N.; Katsaras, J. Model-Based Approaches for the Determination of Lipid Bilayer Structure from Small-Angle Neutron and X-Ray Scattering Data. *Eur. Biophys. J.* **2012**, *41* (10), 875–890. https://doi.org/10.1007/s00249-012-0817-5.

(7) Cheng, X.; Smith, J. C. Biological Membrane Organization and Cellular Signaling. *Chem. Rev.* **2019**, *119* (9), 5849–5880. https://doi.org/10.1021/acs.chemrev.8b00439.

(8) Singer, S. J.; Nicolson, G. L. The Fluid Mosaic Model of the Structure of Cell Membranes. *Science.* **1972**, *175* (4023), 720–731. https://doi.org/10.1126/science.175.4023.720.

(9) Nicolson, G. Update of the 1972 Singer-Nicolson Fluid-Mosaic Model of Membrane Structure. *Discoveries* **2013**. 1, e3. https://doi.org/10.15190/d.2013.3.

(10) Gagnon, M. C.; Dautrey, S.; Bertrand, X.; Auger, M.; Paquin, J. F. A Flexible Synthetic Approach to Phosphatidylglycerols. *Eur. J. Org. Chem.* **2017**, *2017* (43), 6401–6407. https://doi.org/10.1002/ejoc.201701178.

(11) Singer, S. J. A Fluid Lipid-Globular Protein Mosaic Model of Membrane Structure. *Ann. N. Y. Acad. Sci.* **1972**, *195* (1), 16–23. https://doi.org/10.1111/j.1749-6632.1972.tb54780.x.

(12) Zhang, Y. M.; Rock, C. O. Membrane Lipid Homeostasis in Bacteria. *Nat. Rev. Microbiol.* **2008**, *6* (3), 222–233. https://doi.org/10.1038/nrmicro1839.

(13) Edidin, M. Lipids on the Frontier: A Century of Cell-Membrane Bilayers. *Nat. Rev. Mol. Cell Biol.* **2003**, *4* (5), 414–418. https://doi.org/10.1038/nrm1102.

(14) Simons, K.; Toomre, D. Lipid Rafts and Signal Transduction. *Nat. Rev. Mol. Cell Biol.* **2000**, *1* (1), 31-39. https://doi.org/10.1038/35036052.

(15) Simons K. Lipid Rafts: A Personal Account. In *Bassereau P., Sens P., (eds);* Physics of Biological Membranes, Springer, Cham. 2018; pp 109–123. https://doi.org/10.1007/978-3-030-00630-3_4.

(16) Simons, K.; van Meer, G. Lipid Sorting in Epithelial Cells. *Biochemistry*, **1988**, *27* (17), 6197–6202. https://doi.org/10.1021/bi00417a001.

(17) Simons, K.; Ikonen, E. Functional Rafts in Cell Membranes. *Nature,* **1997**, *387* (6633), 569–572. https://doi.org/https://doi. org/10.1038/42408.

(18) Nickels, J. D.; Chatterjee, S.; Stanley, C. B.; Qian, S.; Cheng, X.; Myles, D. A. A.; Standaert, R. F.; Elkins, J. G.; Katsaras, J. The in Vivo Structure of Biological Membranes and Evidence for Lipid Domains. *PLoS Biol.* **2017**, *15* (5), 1-22. https://doi.org/10.1371/journal.pbio.2002214.

(19) Eibl, H. Phospholipids as Functional Constituents of Biomembranes. *Angew. Chem., Int. Ed. Engl.* **1984**, *23* (4), 257–271. https://doi.org/10.1002/anie.198402573.

(20) Pick, H.; Alves, A. C.; Vogel, H. Single-Vesicle Assays Using Liposomes and Cell-Derived Vesicles: From Modeling Complex Membrane Processes to Synthetic Biology and Biomedical Applications. *Chem. Rev.* **2018**, *118* (18), 8598–8654. https://doi.org/10.1021/acs.chemrev.7b00777.

(21) Sohlenkamp, C.; Geiger, O. Bacterial Membrane Lipids: Diversity in Structures and Pathways. *FEMS Microbiol. Rev.* **2015,** *40* (1), 133–159. https://doi.org/10.1093/femsre/fuv008.

(22) Marielle, B.; Sarrah, G. Assessment of Bacterial Membrane Fluidity by Flow Cytometry. *J. Microbiol. Methods* **2017**, *143*, 50–57. https://doi.org/10.1016/j.mimet.2017.10.005.

(23) Denich, T. J.; Beaudette, L. A.; Lee, H.; Trevors, J. T. Effect of Selected Environmental and Physico-Chemical Factors on Bacterial Cytoplasmic Membranes. *J. Microbiol. Methods* **2003**, *52* (2), 149–182. https://doi.org/10.1016/S0167-7012(02)00155-0.

(24) Fonseca, F.; Pénicaud, C.; Tymczyszyn, E. E.; Gómez-Zavaglia, A.; Passot, S. Factors Influencing the Membrane Fluidity and the Impact on Production of Lactic Acid Bacteria

Starters. *Appl. Microbiol. Biotechnol.* **2019**, *103* (17), 6867–6883. https://doi.org/10.1007/s00253-019-10002-1.

(25) Qin, S. S.; Yu, Z. W.; Yu, Y. X. Structural Characterization on the Gel to Liquid-Crystal Phase Transition of Fully Hydrated DSPC and DSPE Bilayers. *J. Phys. Chem. B* **2009**, *113* (23), 8114–8123. https://doi.org/10.1021/jp808779r.

(26) Harb, F.; Simon, A.; Tinland, B. Ripple Formation in Unilamellar-Supported Lipid Bilayer Revealed by FRAPP. *Eur. Phys. J. E: Soft Matter Biol. Phys.* **2013**, *36* (12), 140. https://doi.org/10.1140/epje/i2013-13140-x.

(27) Vereb, G.; Szöllosi, J.; Matkó, J.; Nagy, P.; Farkas, T.; Vígh, L.; Mátyus, L.; Waldmann, T. A.; Damjanovich, S. Dynamic, Yet Structured: The Cell Membrane Three Decades after the Singer-Nicolson Model. *Proc. Natl. Acad. Sci. U. S. A.* **2003**, *100* (14), 8053–8058. https://doi.org/10.1073/pnas.1332550100.

(28) Kučerka, N.; Holland, B.; Pan, J.; Heberle, F. A.; Gray, C. G.; Tomberli, B.; Katsaras, J. The Detailed Scattering Density Profile Model of PG Bilayers as Determined by Molecular Dynamics Simulations, and Small-Angle Neutron and X-Ray Scattering Experiments. *Biophys. J.* **2012**, *102* (3), 504a–505a. https://doi.org/10.1016/j.bpj.2011.11.2764.

(29) Kučerka, N.; Holland, B. W.; Gray, C. G.; Tomberli, B.; Katsaras, J. Scattering Density Profile Model of POPG Bilayers as Determined by Molecular Dynamics Simulations and Small-Angle Neutron and x-Ray Scattering Experiments. *J. Phys. Chem. B* **2012**, *116* (1), 232–239. https://doi.org/10.1021/jp208920h.

(30) Pan, J.; Heberle, F. A.; Tristram-Nagle, S.; Szymanski, M.; Koepfinger, M.; Katsaras, J.; Kučerka, N. Molecular Structures of Fluid Phase Phosphatidylglycerol Bilayers as

Determined by Small Angle Neutron and X-Ray Scattering. *Biochim. Biophys. Acta, Biomembr.* **2012**, *1818* (9), 2135–2148. https://doi.org/10.1016/j.bbamem.2012.05.007.

(31) Kučerka, N.; Nagle, J. F.; Sachs, J. N.; Feller, S. E.; Pencer, J.; Jackson, A.; Katsaras, J. Lipid Bilayer Structure Determined by the Simultaneous Analysis of Neutron and X-Ray Scattering Data. *Biophys. J.* **2008**, *95* (5), 2356–2367. https://doi.org/10.1529/biophysj.108.132662.

(32) Kučerka, N.; Nieh, M. P.; Katsaras, J. Fluid Phase Lipid Areas and Bilayer Thicknesses of Commonly Used Phosphatidylcholines as a Function of Temperature. *Biochim. Biophys. Acta, Biomembr.* **2011**, *1808* (11), 2761–2771. https://doi.org/10.1016/j.bbamem.2011.07.022.

(33) Cronan, J. E.; Gelmann, E. P. Physical Properties of Membrane Lipids: Biological Relevance and Regulation. *Bacteriol. Rev.* **1975**, *39* (3), 232–256. https://doi.org/10.1128/mmbr.39.3.232-256.1975.

(34) Weber, G.; Farris, F. J. Synthesis and Spectral Properties of a Hydrophobic Fluorescent Probe: 6-Propionyl-2-(dimethylamino)naphthalene. *Biochemistry.* **1979**, *18* (14), 3075–3078. doi:10.1021/bi00581a025.

(35) Bagatolli L.A. The Lateral Structure of Lipid Membranes as Seen by Fluorescence Microscopy. In *Hof M., Hutterer R., Fidler V.*, (eds); Fluorescence Spectroscopy in Biology. Springer Series on Fluorescence (Methods and Applications), Vol. 3; Springer, Berlin, Heidelberg, 2005; pp 150–159. https://doi.org/10.1007/3-540-27004-3_9.

(36) Parasassi, T.; Krasnowska, E. K.; Bagatolli, L.; Gratton, E. Laurdan and Prodan as Polarity-Sensitive Fluorescent Membrane Probes. *J. Fluoresc.* **1998**, *8* (4), 367–373. https://doi.org/10.1023/A:1020528716621.

(37) Rodionova, M. V.; Poudyal, R. S.; Tiwari, I.; Voloshin, R. A.; Zharmukhamedov, S. K.; Nam, H. G.; Zayadan, B. K.; Bruce, B. D.; Hou, H. J. M.; Allakhverdiev, S. I. Biofuel Production: Challenges and Opportunities. *Int. J. Hydrogen Energy* **2017**, *42* (12), 8450–8461. https://doi.org/10.1016/j.ijhydene.2016.11.125.

(38) Machado, I. M. P.; Atsumi, S. Cyanobacterial Biofuel Production. *J. Biotechnol.* **2012**, *162* (1), 50–56. https://doi.org/10.1016/j.jbiotec.2012.03.005.

(39) Kour D. et al. Technologies for Biofuel Production: Current Development, Challenges, and Future Prospects. In *Rastegari A., Yadav A., Gupta A.* (eds); Prospects of Renewable Bioprocessing in Future Energy Systems. Biofuel and Biorefinery Technologies, Vol 10. Springer, Cham., 2019; pp 1–50. https://doi.org/10.1007/978-3-030-14463-0_1.

(40) Peralta-Yahya, P. P.; Keasling, J. D. Advanced Biofuel Production in Microbes. *Biotechnol. J.* **2010**, *5* (2), 147–162. https://doi.org/10.1002/biot.200900220.

(41) Shanahan, R. M.; Hickey, A.; Bateman, L. M.; Light, M. E.; McGlacken, G. P. One-Pot Cross-Coupling/C-H Functionalization Reactions: Quinoline as a Substrate and Ligand through N-Pd Interaction. *J. Org. Chem.* **2020**, *85* (4), 2585–2596. https://doi.org/10.1021/acs.joc.9b03321.

(42) Sanderson, K. Lignocellulose: A Chewy Problem. *Nature* **2011**, *474* (7352), S12–S14. https://doi.org/10.1038/474S012a.

(43) Ohkuma, M.; Noda, S.; Hattori, S.; Iida, T.; Yuki, M.; Starns, D.; Inoue, J. I.; Darby, A. C.; Hongoh, Y. Acetogenesis from H_2 plus CO_2 and Nitrogen Fixation by an Endosymbiotic Spirochete of a Termite-Gut Cellulolytic Protist. *Proc. Natl. Acad. Sci. U. S. A.* **2015**, *112* (33), 10224–10230. https://doi.org/10.1073/pnas.1423979112.

(44) Inoue, T.; Moriya, S.; Ohkuma, M.; Kudo, T. Molecular Cloning and Characterization of a Cellulase Gene from a Symbiotic Protist of the Lower Termite, *Coptotermes formosanus*. *Gene* **2005**, *349*, 67–75. https://doi.org/10.1016/j.gene.2004.11.048.

(45) Wang, X.; Yomano, L. P.; Lee, J. Y.; York, S. W.; Zheng, H.; Mullinnix, M. T.; Shanmugam, K. T.; Ingram, L. O. Engineering Furfural Tolerance in *Escherichia coli* Improves the Fermentation of Lignocellulosic Sugars into Renewable Chemicals. *Proc. Natl. Acad. Sci. U. S. A.* **2013**, *110* (10), 4021–4026. https://doi.org/10.1073/pnas.1217958110.

(46) Smith, M. D.; Pingali, S. V.; Elkins, J. G.; Bolmatov, D.; Standaert, R. F.; Nickels, J. D.; Urban, V. S.; Katsaras, J.; Davison, B. H.; Smith, J. C.; Petridis, L. Solvent-Induced Membrane Stress in Biofuel Production: Molecular Insights from Small-Angle Scattering and All-Atom Molecular Dynamics Simulations. *Green Chem.* **2020**, *22* (23), 8278–8288. https://doi.org/10.1039/D0GC01865A.

(47) Cheng, X.; Smith, J. C. Biological Membrane Organization and Cellular Signaling. *Chem. Rev.* **2019**, *119* (9), 5849–5880. https://doi.org/10.1021/acs.chemrev.8b00439.

(48) Saeui, C.; Mathew, M.; Liu, L.; Urias, E.; Yarema, K. Cell Surface and Membrane Engineering: Emerging Technologies and Applications. *J. Funct. Biomater.* **2015**, *6* (2), 454–485. https://doi.org/10.3390/jfb6020454.

(49) Mentewab, A.; Stewart, C. N. Overexpression of an *Arabidopsis thaliana* ABC Transporter Confers Kanamycin Resistance to Transgenic Plants. *Nat. Biotechnol.* **2005**, *23* (9), 1177–1180. https://doi.org/10.1038/nbt1134.

(50) Yu, L.; Gupta, S.; Xu, F.; Liverman, A. D. B.; Moschetta, A.; Mangelsdorf, D. J.; Repa, J. J.; Hobbs, H. H.; Cohen, J. C. Expression of ABCG5 and ABCG8 Is Required for

Regulation of Biliary Cholesterol Secretion. *J. Biol. Chem.* **2005**, *280* (10), 8742–8747. https://doi.org/10.1074/jbc.M411080200.

(51) Pighin, J. A. Plant Cuticular Lipid Export Requires an ABC Transporter. *Science* **2004**, *306* (5696). https://doi.org/10.1126/science.1102331.

(52) Lewis, A. R.; Reber, K. P. Synthesis of Antifungal Alatanone and Trineurone Polyketides. *Tetrahedron Lett.* **2016**, *57* (10), 1083–1086. https://doi.org/10.1016/j.tetlet.2016.01.090.

(53) Baer, T. A.; Carney, R. L. Copper Catalyzed Reaction of Grignard Reagents with Chloromagnesium Salts of ω-Bromoacids. *Tetrahedron Lett.* **1976**, *17* (51), 4697–4700. https://doi.org/10.1016/S0040-4039(00)92999-X.

(54) Lindberg, J.; Ekeroth, J.; Konradsson, P. Efficient Synthesis of Phospholipids from Glycidyl Phosphates. *J. Org. Chem.* **2002**, *67* (1), 194–199. https://doi.org/10.1021/jo010734+.

(55) Kruizinga, W. H.; Strijtveen, B.; Kellogg, R. M. Cesium Carboxylates in Dimethyl Formamide. Reagents for Introduction of Hydroxyl Groups by Nucleophilic Substitution and for Inversion of Configuration of Secondary Alcohols. *J. Org. Chem.* **1981**, *46* (21) 4321–4323. https://doi.org/10.1021/jo00334a055.

(56) Makita, A.; Yamada, Y.; Okada, H. The Total Synthesis of (±)-Patulolide A. *J. Antibiot.* **1986**, *39* (9) 1257–162. https://doi.org/10.7164/antibiotics.39.1257.

(57) Novotný, J.; Pospěchová, K.; Hrabálek, A.; Čáp, R.; Vávrová, K. Synthesis of Fluorescent C_{24}-Ceramide: Evidence for Acyl Chain Length Dependent Differences in Penetration of Exogenous NBD-Ceramides into Human Skin. *Bioorg. Med. Chem. Lett.* **2009**, *19* (24), 6975–6977. https://doi.org/10.1016/j.bmcl.2009.10.047.

(58) Kim Ha, J.; Lindsay, R. C. Mass Spectra of Butyl Esters of Volatile Branched-Chain and Other Fatty Acids Occurring in Milkfat and Meat Lipids. *J. Food Compos. Anal.* **1989**, *2* (2), 118–131. https://doi.org/10.1016/0889-1575(89)90072-0.

(59) Richardson, M. B.; Williams, S. J. A practical synthesis of long-chain iso-fatty acids (iso-C_{12}–C_{19}) and related natural products. *Beilstein J. Org. Chem.* **2013,** 9, 1807–1812. https://doi.org/10.3762/bjoc.9.210.

(60) Parasassi, T.; Giusti, A. M.; Gratton, E.; Monaco, E.; Raimondi, M.; Ravagnan, G.; Sapora, O. Evidence for an Increase in Water Concentration in Bilayers after Oxidative Damage of Phospholipids Induced by Ionizing Radiation. *Int. J. Radiat. Biol.* **1994**, *65* (3), 329–334. https://doi.org/10.1080/09553009414550391.

APPENDIX: ^{1}H NMR Spectrum of Impure 13-Methyltetradecanoic Acid

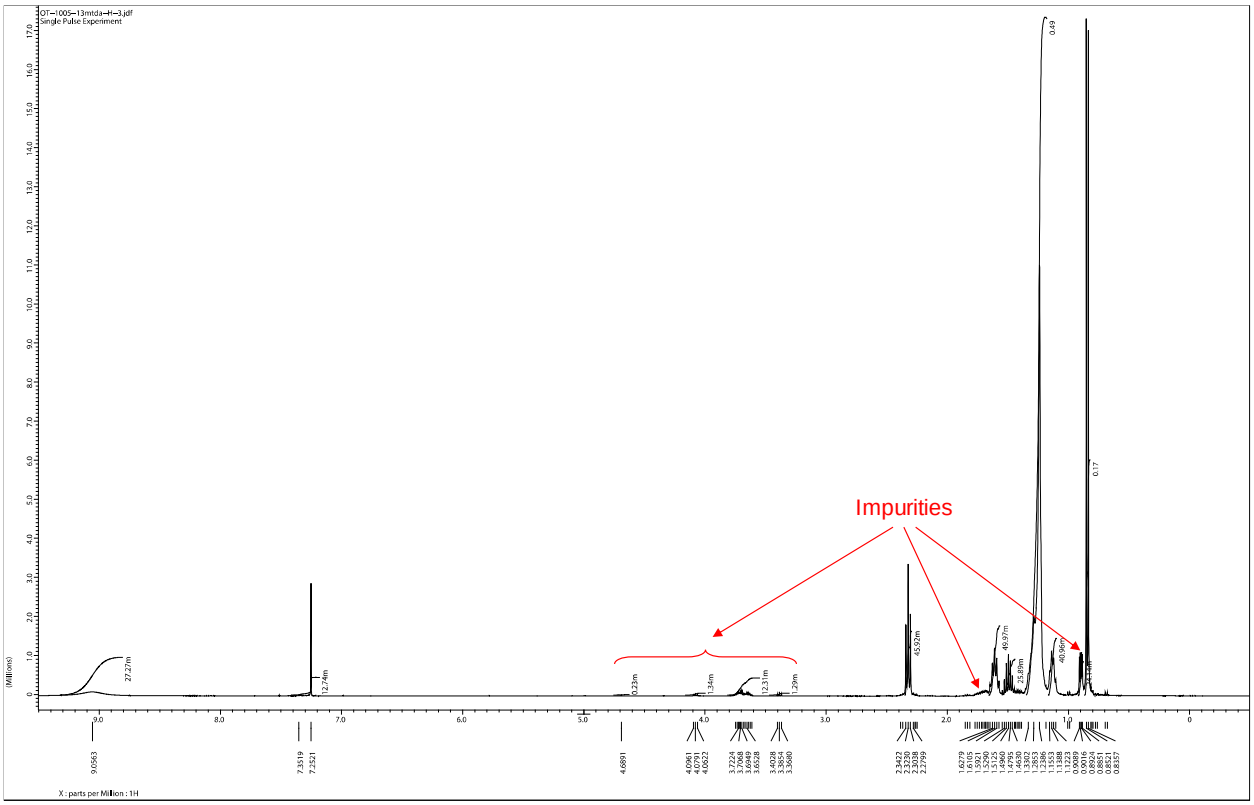

VITA

JOHN HAYFORD G. TEYE-KAU

Education:	M.S. Chemistry, East Tennessee State University, Johnson City, Tennessee, 2021
	B.Sc. Applied Chemistry, University for Development Studies, Navrongo, Tamale, Ghana 2013
Professional Experience:	Laboratory Intern, Water Quality Unit, Volta River Authority, Akosombo, Ghana, 2012
	Laboratory Technologist, Nuclear Chemistry and Environmental Research Centre, Ghana Atomic Energy Commission, Kwabenya, Accra, Ghana, 2013-2015
	Quality Control Officer, Geo Medicore Limited, Kuntunse, Accra, Ghana, 2015-2016
	Manager, Christ Cooperative Credit Union, Adenta, Accra, Ghana, 2016-2019
	Graduate Assistant, East Tennessee State University, College of Arts and Sciences, 2019-2021
Honors and Awards:	2nd Place, ETSU 3MT®, Fall 2020
	Member, American Chemical Society, Admitted 2021
	Member, Graduate and Professional Student Association (GPSA), East Tennessee State University, 2019-2021